



Tectonics

RESEARCH ARTICLE

10.1029/2017TC004906

Key Points:

- High-resolution 3-D seismic data indicate widespread normal faulting on the upper slope of the northeastern Hikurangi margin
- The normal faults show two major strike directions, primarily landward dip, low vertical displacements, and steep dip angles
- Extension may be controlled by regional uplift or/and extensional strain due to rotation of tectonic blocks around nearby poles

Correspondence to:

C. Böttner,
cboettner@geomar.de

Citation:

Böttner, C., Gross, F., Geersen, J., Crutchley, G. J., Mountjoy, J. J., & Krastel, S. (2018). Marine forearc extension in the Hikurangi margin: New insights from high-resolution 3-D seismic data. *Tectonics*, 37, 1472–1491. <https://doi.org/10.1029/2017TC004906>

Received 6 DEC 2017

Accepted 17 APR 2018

Accepted article online 26 APR 2018

Published online 21 MAY 2018

Marine Forearc Extension in the Hikurangi Margin: New Insights From High-Resolution 3-D Seismic Data

Christoph Böttner^{1,2} , Felix Gross¹ , Jacob Geersen² , Gareth J. Crutchley³ , Joshu J. Mountjoy⁴ , and Sebastian Krastel¹ 

¹Institute of Geosciences, Christian-Albrechts-Universität zu Kiel, Kiel, Germany, ²GEOMAR Helmholtz Centre for Ocean Research Kiel, Kiel, Germany, ³GNS Science, Lower Hutt, New Zealand, ⁴NIWA, Wellington, New Zealand

Abstract Upper-plate normal faults are a widespread structural element in erosive plate margins. Increasing coverage of marine geophysical data has proven that similar features also exist in accretionary margins where horizontal compression usually results in folding and thrust faulting. There is a general lack of understanding of the role and importance of normal faulting for the structural and tectonic evolution of accretionary margins. Here we use high-resolution 2-D and 3-D seismic reflection data and derived seismic attributes to map and analyze upper-plate normal faulting in the marine forearc of the accretionary Hikurangi margin, New Zealand. We document extension of the marine forearc over a wide area along the upper continental slope. The seismically imaged normal faults show low vertical displacements, high dip angles, a preference for landward dip, and often an echelon patterns. We evaluate different processes, which may cause the observed extension, including (1) stress change during the earthquake cycle, (2) regional or local uplift and decoupling of shallow strata from compression at depth, and (3) rotation of crustal blocks and resulting differential stresses at the block boundaries. The results suggest that normal faults play an important role in the structural and tectonic evolution of accretionary margins, including the northern Hikurangi forearc.

1. Introduction

In subduction zones, upper-plate normal faults have long been considered a tectonic feature primarily associated with erosive margins. However, increasing coverage of marine seismic data has proven that similar features also exist in accretionary margins, such as Cascadia (McNeill et al., 1997), Makran (Grando & McClay, 2007), Nankai (Gulick et al., 2010; Moore et al., 2013), or Central Chile (Geersen et al., 2011, 2016), where kinematics are dominated by compression. In addition, extensional aftershocks in the overriding plate have been documented in the wake of recent large megathrust earthquakes, including the 2010 Chile (*Mw* 8.8) and 2011 Japan (*Mw* 9.0) events (Asano et al., 2011; Fariás et al., 2011; Ide et al., 2011). After being recognized in many accretionary subduction zones, there is currently much debate about the role and importance of normal faults and zones of extension in these settings. This includes not only their role for the seismotectonic evolution of an accretionary margin but also the seismic and tsunami hazard they pose, as well as their impact on fluid flow and fluid seepage.

Different models have been evoked to explain extension in accretionary margins. These models include (1) regional uplift due to basal underplating of subducted sediment or shortening across upper-plate thrust faults (e.g., Gulick et al., 2010), (2) local uplift due to subduction of excess topography on the oceanic plate (Masson et al., 1990; Ranero & von Huene, 2000), (3) mechanical decoupling of the shallow forearc strata from the underlying compressional subduction regime along a crustal décollement (Buck & Sokoutis, 1994; McNeill et al., 1997; Moore et al., 2013; Zoback et al., 1981), and (4) dominance and prevalence of extensional strain during the coseismic or early postseismic phase of a megathrust earthquake (Aron et al., 2013; Cubas, Avouac, Leroy, & Pons, 2013; Cubas, Avouac, Souloumiac, & Leroy, 2013).

For the Hikurangi margin off the North Island of New Zealand (Figure 1), geodetic data and structural investigations have revealed normal faulting in parts of the terrestrial forearc (Cashman & Kelsey, 1990; Mazengarb, 1984; Walcott, 1978, 1987). In the offshore forearc, normal faults have been imaged locally around the crests of slope-parallel ridges by means of seismic reflection and multibeam bathymetric data (Kukowski et al., 2010; Plaza-Faverola et al., 2014). However, little is known about how large-scale upper-

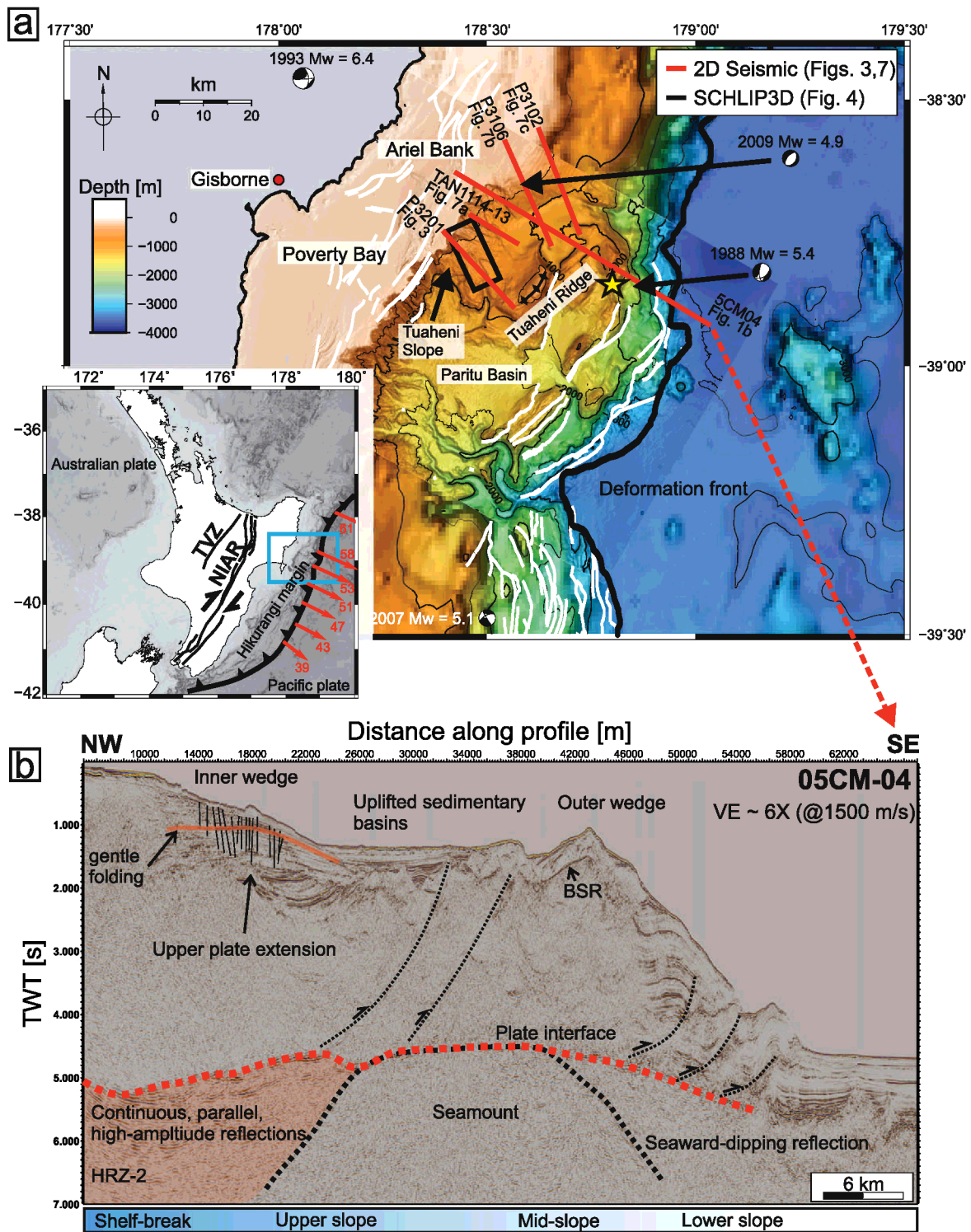


Figure 1. (a) Map of the northern Hikurangi margin composed of GEBCO and high-resolution bathymetry (100-m grid, source: NIWA). Focal mechanisms are taken from the global CMT catalog (Dziewonski et al., 1981; Ekström et al., 2012), and the location of the 1947 Poverty Bay earthquake is indicated with a yellow star (after Bell et al., 2014). The small inset shows location of the area of study within respect to the Australian and Pacific Plates. Red vectors show long-term convergence at the Hikurangi trench in millimeter per year (modified after Wallace et al., 2004 and Wallace et al., 2009). White lines image active faults within the region (source: NIWA). TVZ = Taupo volcanic zone; NIAR = North Island axial ranges. (b) Interpreted seismic reflection profile 05CM-04 located at the northern Hikurangi Margin off Gisborne, New Zealand, with seismic interpretations after Bell et al. (2010) (HRZ-2 = high-amplitude reflectivity zone 2). Red line highlights gentle folding of upper-plate strata. The location of the profile is shown in (a) and vertical exaggeration is ~ 6 times at 1,500 m/s. NIWA = National Institute of Water and Atmospheric Research; BSR = bottom-simulating reflection; TWT = two-way travel time.

plate extension in the terrestrial forearc continues offshore into the marine forearc. Here we combine regional 2-D seismic reflection lines and a high-resolution 3-D seismic volume from the upper slope of the northern Hikurangi margin in the area of Tuaheni Slope (off the coast from Gisborne) to map and analyze normal faulting in the marine forearc. Based on the structural investigations, we consider the mechanisms that control upper-plate extension.

1.1. Geological Setting of the Hikurangi Margin

The Hikurangi margin, located off the East Coast of the North Island of New Zealand, is shaped by the subduction of the Pacific Plate beneath the Australian Plate (Figure 1). It represents the transition from Tonga-Kermadec subduction to the north to continental collision and the strike-slip Alpine fault farther south (Nicol et al., 2007). The rate of plate convergence decreases from 60 mm/a in the north to 30 mm/a in the south (Beavan et al., 2002; Wallace et al., 2004). Convergence occurs oblique toward the SW (Beavan et al., 2002). The oblique convergence separates into a margin-normal component, accommodated in the subduction thrust, and a margin-parallel component, mainly accommodated across the North Island Axial Ranges (dextral shear zone) and by clockwise rotation of the eastern North Island (Beanland & Haines, 1998; Nicol & Wallace, 2007; Wallace et al., 2004; Webb & Anderson, 1998). Geodetic measurements indicate a segmentation of the Australian Plate in the region of the North Island into individual tectonic blocks (Nicol & Wallace, 2007; Wallace et al., 2004). The southward decrease in convergence along the margin results in clockwise rotation of the tectonic blocks around poles located to the west of the North Island (Mumme et al., 1989; Walcott, 1984; Wallace et al., 2004). The stresses that result from rotation of the individual blocks are mainly accommodated along interconnected faults along the block boundaries (McCaffrey, 2002; McCaffrey et al., 2000; McClusky et al., 2001; Wallace et al., 2004). Intra-arc extension occurs within the Taupo volcanic zone as a result of rapid rotation of the North Island forearc (Nicol & Wallace, 2007; Wallace et al., 2004).

The structure and geometry of the Hikurangi margin, including the nature of the plate boundary, vary along the margin (Barker et al., 2009; Bell et al., 2010; Reyners, 1998; Wallace et al., 2004). Crustal thickness of the Pacific Plate along the trench increases from 10–15 km in the north to 20–25 km at the Chatham Rise (Davy & Wood, 1994). Frontal accretion of trench sediments results in the formation of an active accretionary prism with predominantly landward-dipping prism thrust faults. The frontal part of the accretionary prism takes up about 90% of the margin normal component of plate convergence (Pedley et al., 2010). In addition to horizontal shortening and thrust faulting, the geomorphology and structural evolution of the Hikurangi margin is further influenced by the subduction of several seamounts on the oceanic plate as well as gravitationally driven sediment transport processes and resulting mass transport deposits (MTDs; Bell et al., 2010; Mountjoy et al., 2009, 2014; Mountjoy & Barnes, 2011; Pedley et al., 2010).

1.2. Local Geological Setting

This study is located in the area of Tuaheni Slope (Figure 1a). The tectonic setting and margin geometry have been described and analyzed by Barker et al. (2009) and Bell et al. (2010) based on margin orthogonal 2-D seismic reflection data such as line 05CM-04 (compare Figure 1b). Line 05CM-04 images the plate interface to 50-km landward of the deformation front. The outermost accretionary wedge shows high slope angles (up to 10°) suggesting oversteepening (Barker et al., 2009). The margin is locally modified by the subduction of a seamount (Figure 1b). At depth, the landward section of the subducting seamount shows continuous, parallel, high-amplitude reflections, which Bell et al. (2010) defined as high-amplitude reflectivity zone 2 (HRZ-2). The seismic section reveals a bottom-simulating reflection (BSR), which is visible from the upper slope to lower slope (Figure 1b). At the upper continental slope, Tuaheni Ridge forms the lower boundary of an upper-slope basin. In this area the upper-slope basins are uplifted, possibly due to upper-plate contractional faulting (Berryman et al., 1989; Ota & Yamaguchi, 2004), underplating (Reyners & McGinty, 1999; Walcott, 1987), and/or seamount subduction during the last 2 Ma (Bell et al., 2010; Pedley et al., 2010). The continental shelf is dominated by Ariel Bank fault, which shows vertical slip rates of up to 3–5 mm/year (Mountjoy & Barnes, 2011). However, the activity of upper-plate faults underlying the middle and upper continental slope is usually not well constrained (Bell et al., 2010; Mountjoy & Barnes, 2011).

Two major geological units make up the sedimentary succession at Tuaheni Slope. The lower unit consists of Miocene to Pliocene rock, partly exposed by erosion and tectonic uplift, for example, Tuaheni ridge,

with possible Cretaceous and Paleogene sedimentary rocks at depth (Barnes et al., 2002, 2010, Field & Uruski, 1997; Mountjoy & Barnes, 2011; Pedley et al., 2010). The upper unit consists of Quaternary shelf-edge low-stand clinoform sequences from the outer shelf to the upper slope. These clinoform sequences developed during a eustatic low of the sea level due to glacial cycles (Catuneanu et al., 2009; Van Wagoner et al., 1988). Holocene sedimentation formed fine-grained clinoform sequences southwest of Tuaheni Slope, with intercalated sand fractions (Alexander et al., 2010; Barnes et al., 1991). A similar sedimentary succession is likely present at Tuaheni Slope (Mountjoy et al., 2014). The upper slope shows indications for upper-plate extension within the first 0.5-s two-way travel time (TWT) of the sedimentary succession (Figure 1b).

Most earthquakes of the offshore northern Hikurangi margin are associated with thrust faulting. Peak ground acceleration of 0.4–0.5 g is expected at a recurrence rate of about 250 years, according to the New Zealand National Seismic Hazard Model (Stirling et al., 2012). Over the past century, the margin experienced a series of tsunamogenic earthquakes (Fraser, 1998) including one in 1931 ($M_w \sim 7.9$) near Napier/Hawke Bay (Conly, 1980; De Lange & Healy, 1986) and two in 1947 ($M_w 7.0$ – 7.1 , yellow star in Figure 1a, and $M_w 6.9$ – 7.1) off Gisborne (Bell et al., 2014; De Lange & Healy, 1986). These events caused 6- to 10-m runup heights, damage to shore-based structures, damage, and loss of floating objects and flooding of coastal regions (De Lange & Healy, 1986). During the last ~ 30 years, four earthquakes (1988, 1993, 2007, and 2009) occurred at depths less than 20 km indicating that they likely originated in the upper plate (Dziewonski et al., 1981; Ekström et al., 2012). The four earthquakes had magnitudes ranging from 4.9 to 6.4 M_w and were of normal to strike-slip character (Figure 1a).

2. Materials and Methods

2.1. Seismic Data—SCHLIP3D and 2-D

In this study we use a combination of high-resolution 2-D and 3-D seismic reflection data. Most of the seismic data were acquired during RV *Tangaroa* cruise TAN1404 in April 2014.

During survey TAN1404, the 2-D seismic system consisted of a 0.7-l GI Gun and a 150-m long streamer with 96 channels; channel spacing was 1.5625 m. Processing included crooked line common midpoint (CMP) binning at a spacing of 1.5 m, a Butterworth-type frequency filter (10/35 to 150/200 Hz), normal moveout correction with constant velocity of 1,500 m/s, stacking, and a 2-D Stolt time migration with a constant velocity of 1,500 m/s. From the TAN1404 data set, we use seismic lines P3106, P3406, and P3102 (Figure 1a). In addition, we use seismic line TAN1114-13 which was acquired during RV *Tangaroa* cruise TAN1114 (2011) using a 600-m long streamer with 48 channels at 12.5-m spacing, and 2×0.7 l/1.7 l GI guns (Barnes et al., 2011; Mountjoy et al., 2014).

Three-dimensional seismic data were also collected during cruise TAN1404 using the 3-D P-cable system. The system consists of a cross cable towed behind the ship in between two paravanes. The cross cable approximately forms the shape of a catenary as it is towed through the water, with the end points (at the paravanes) spanning a distance of ~ 150 m. The catenary form enables a predictive calculation of receiver array positions given the known end points (the paravanes equipped with GPS), the length of the cable, and the ship's azimuth. These predicted receiver positions were refined using the direct wave arrival times at each streamer channel. During cruise TAN1404, the P-cable system consisted of 15 streamer segments, each ~ 12.5 -m long, with eight channels at a spacing of 1.5625 m. The 0.7-l GI Gun was towed ~ 30 m behind the ship, shot every 3 s, and had frequencies between 15 and 400 Hz. This small shot interval (equating to ~ 5 m at 3.5 knots sailing speed) enabled dense CMP binning onto a grid with a 3.125-m CMP spacing. Processing included band-pass filtering (40/70 to 350/500 Hz), CMP stacking, stacking of successive inlines to reduce data gaps (resulting in a 6.25-m inline spacing while maintaining the 3.125-m crossline spacing), normal moveout correction with a constant velocity (1500 m/s), and despiking. We ran a 2-D trace interpolation, first in the crossline direction then in the inline direction, to fill small data gaps in the 3-D seismic volume. Finally, we migrated the volume with a 3-D poststack Kirchhoff time migration using a constant velocity of 1500 m/s and an aperture of 500 m. The resulting seismic volume is ~ 13.5 -km long and ~ 5.9 -km wide. We hereafter refer to the 3-D seismic volume as SCHLIP3D (the acronym of the project named "Submarine Clathrate Hydrate Landslide Imaging Project in 3-D" under which the data were acquired).

2.2. Seismic Attribute Analyses

2.2.1. Fault Detection With Attributes

Bahorich and Farmer (1995) introduced the use of attributes (coherence) to seismic interpretation to enhance the interpretation of seismic sections. Faults are visible in seismic data as a clear displacement of adjacent reflections. Seismic attributes make use of this discontinuity and therefore provide a powerful and reliable tool for fault detection within 3-D seismic volumes (e.g., Moore et al., 2013; Neves et al., 2004). Crucial to a proper analysis are well-interpreted seismic horizons, which avoid the issue of discontinuities induced by the intersection of time slices with stratigraphic layering. Common attributes use either physical or geometrical properties of the complex seismic trace (Taner et al., 1979), for example, similarity (Bahorich & Farmer, 1995). Here we favor and apply visual attributes (Symmetry and derivative Illuminator 3-D [I3D] volumes) introduced by IHS Kingdom. These attributes provide a clear image of deformation patterns and fault planes, offer high resolution, and show a good signal-to-noise ratio at all depth levels and horizons (Yu et al., 2015).

2.2.2. Symmetry (I3D Attributes)

Symmetry is a newly designed poststack, postmigration structural feature detection tool (e.g., fault detection) based on a 3-D log-Gabor filter array (Yu et al., 2015) introduced by IHS within their Kingdom software. It represents a new type of seismic attribute for 3-D data analysis, which is referred to as visual attributes. Symmetry is inspired by neuronal mechanisms of visual perception for orientation patterns. The attribute is sensitive to seismic amplitude variations and hence correlates with discontinuities and curvatures associated with geological surfaces. Its strength is to identify faults, fractures, channels, and other discontinuous events.

We used the SCHLIP3D seismic volume for our Symmetry I3D Energy attribute, a derivative volume of the Symmetry attribute (Yu et al., 2015). The algorithm ran with a 100-ms vertical filter window to obtain a better image, resolve only relatively long faults (i.e., longer than 100 ms), and to diminish the influence of noise, for example, from diffraction hyperbolas (Yu et al., 2015; IHS Kingdom 2017 manual).

2.3. Estimation of Fault Dip and Vertical Displacement

We derived the fault dip from fault planes visible in vertical seismic displays (2-D) and attribute horizon slices (3-D). To obtain accurate measurements, we took the topmost and lowermost points to which we could trace the coherent displacement of adjacent traces and measured the vertical and horizontal lengths (Figure 2). With these length measurements perpendicular to the fault strike and basic trigonometric calculations, we were able to estimate the true fault dip. We calculated the vertical displacement from measurements at the top, center, and bottom of the visible fault plane (Figure 2). With these two parameters, we calculated the total horizontal displacement with trigonometric calculations. The resulting estimates give us a good approximation of the extension per unit length without considering the rock parameters.

All these measurements and calculations depend on the applied seismic velocity model. For our analysis, we use a constant velocity of 1,600 m/s, which is a good approximation for water-saturated sediments. The in situ displacements will increase slightly with depth due to higher velocities in deeper strata. An increase to a velocity of 2,000 m/s, which may be representative for sandy interbeds inside the clinofolds (Press, 1966), would result in 25% higher displacement values. Similarly, the dip angle calculations are dependent on the velocities through the tangent function (Figure 2). However, as the velocities only influence the numerator of the calculation the deviations possible from the actual dip angles are relatively small. For example, a fault with a dip angle of 88.4° would change in dip from 88.4° at 1,600 m/s to 88.7° at 2,000 m/s. Increasing velocities with depth are expected in the subsurface, which would cause similar or higher increase in fault angle (e.g., Yielding et al., 1991).

3. Results

3.1. Results From 2-D Seismic Data

High-resolution 2-D seismic line P3201 (Figure 3) extends over 21 km from the shelf break, which represents the transition from Ariel Bank to the headwall of the Tuaheni Landslide Complex (Mountjoy et al., 2009), to the Tuaheni Ridge (Figure 1a). The latter forms the distal boundary of the upper slope (Figure 1a). The western part of the seismic line (3–13.5 km along profile) overlaps with inline 1664 of the 3-D seismic volume shown in Figure 4 and discussed subsequently.

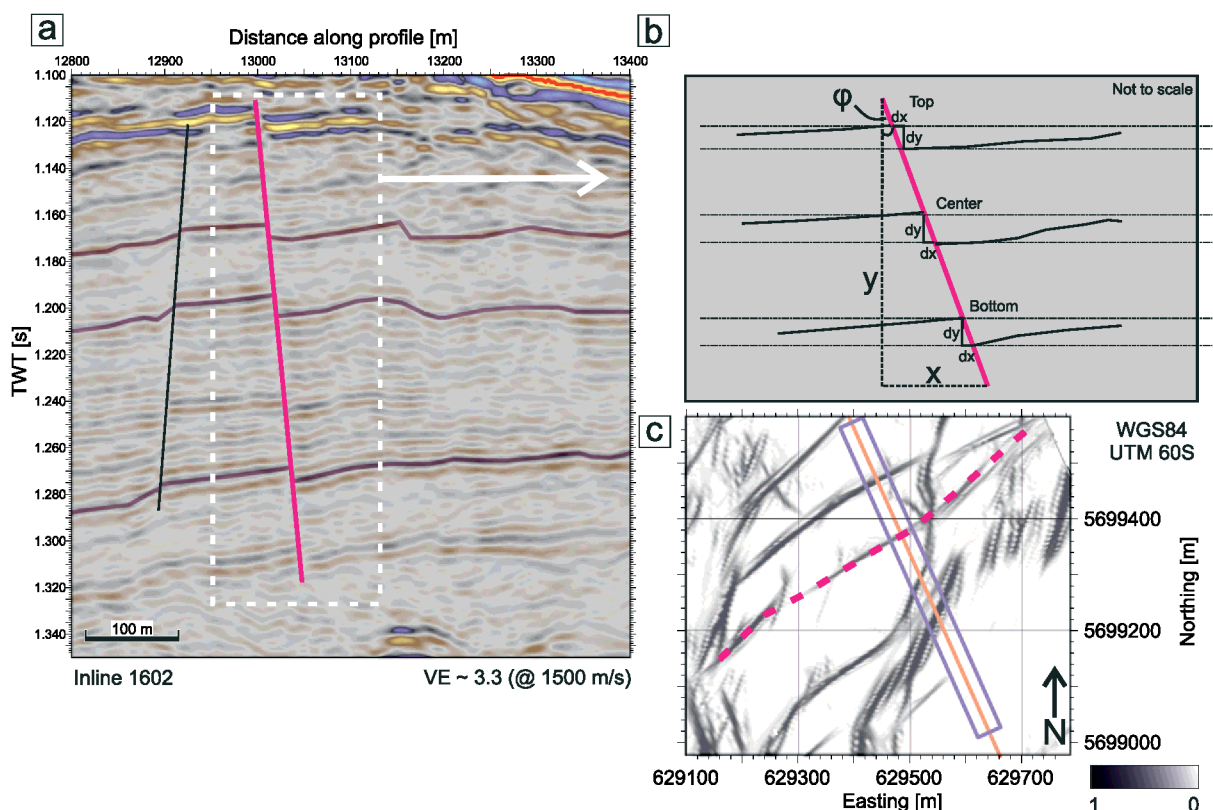


Figure 2. (a) Example arbitrary line from the 3-D seismic volume, highlighting normal faults and the offset reflections. (b) Schematic sketch of the methods applied to determine fault characteristics: Total vertical (x) and horizontal (y) fault extents for dip calculation (ϕ), and three measurements at different depth levels (top, center, and bottom) of horizontal (dx) and vertical (dy) displacement. This sketch is not to scale, in order to emphasize dx/dy measurements. (c) Location within the seismic attribute map (I3D Energy) of the seismic profile displayed in (a). TWT = two-way travel time.

Quaternary clinoforms dominate the seismic image in the western part of line P3201 (Figure 3). The base of gas hydrate stability is manifested in this section as an alignment of truncated high-amplitude reflections, that is, a discontinuous BSR (white arrows in Figure 3b). Between 9 and 18 km along profile, the clinoforms are pervasively intersected by steeply dipping normal faults ($> 65^\circ$), which have vertical offsets in the range of 1- to 19-ms TWT ($\sim 1\text{--}15$ m, assuming a representative velocity of 1,600 m/s). A decreasing signal-to-noise ratio with increasing depth below seafloor prohibits the analysis of these faults below ~ 1.4 -s TWT (10–17 km along profile). The presence of Tuaheni Ridge modifies the sedimentary succession eastward of 14 km along profile. Folded strata that crop out at the seafloor from 19 to 21 km along profile characterize the ridge (Figure 3).

3.2. Results From 3-D Seismic Data

The SCHLIP3D seismic volume extends from the shelf break to Tuaheni Canyon (Figure 1a). It images the upper slope in the area of the southern lobe of the Tuaheni Landslide Complex down to the acoustic basement at 1.5-s TWT. Figure 4 shows inline 1664, which is located adjacent to 2-D line P3201 (3–13.5 km along profile, Figure 3). From 3 to 13.5 km along profile, in the area of the Tuaheni Landslide Complex, the upper 300-ms TWT of the subseafloor shows two different seismic units with chaotic seismic facies, commonly interpreted as MTDs (see Figure 4).

Low-stand clinoforms dominate inline 1664 between 2.2 and 13 km along profile and at TWTs greater than 0.7 s (Figure 4). We pick two characteristic clinoform surfaces (Clinoform A and Clinoform B, Figure 4b) due to their seismic significance with high amplitudes and good lateral continuity. Thereby, we separate the sediments below the MTDs of the Tuaheni Landslide Complex into seismic units A and B. The BSR crosscuts the sedimentary succession from ~ 10 to 13.5 km along profile (Figure 4).

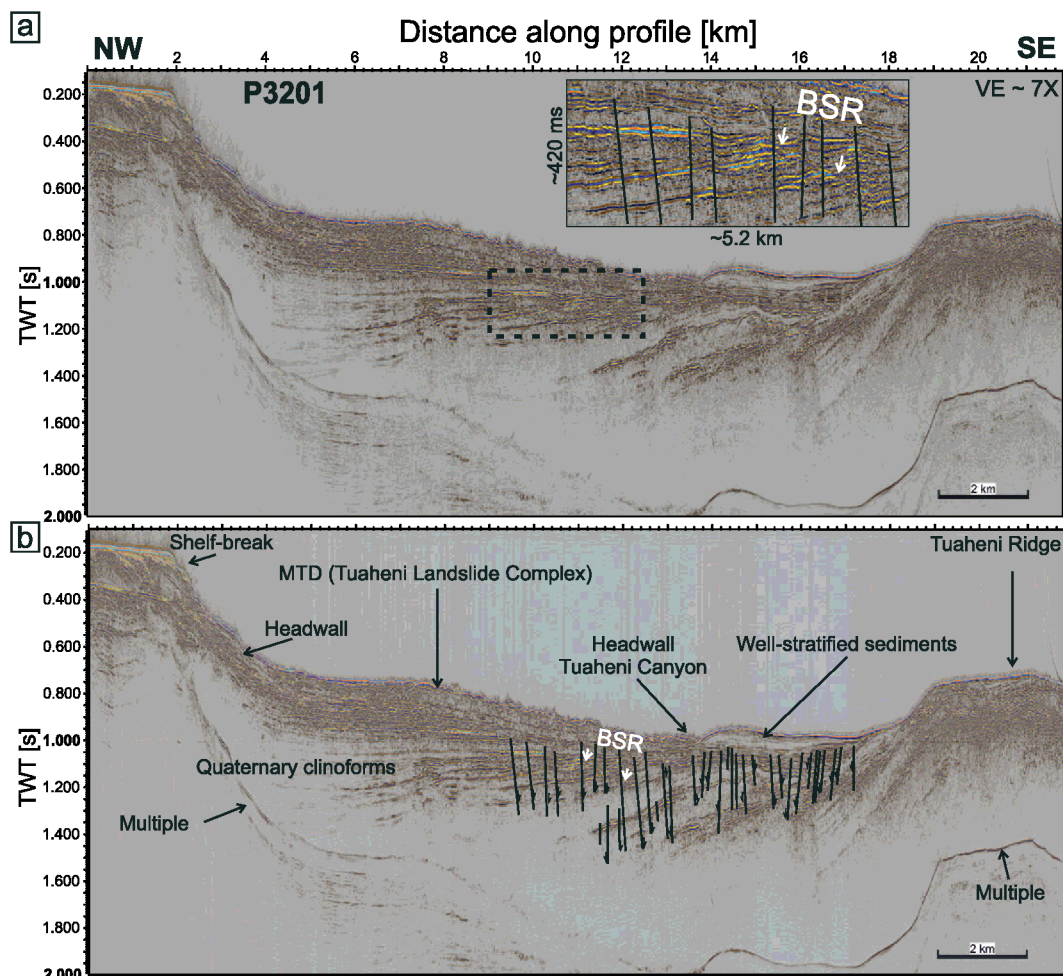


Figure 3. (a) Uninterpreted and (b) interpreted seismic reflection profile P3201 (see Figure 1a for location) showing major geological units. Interpretation of the mass transport deposit (MTD) is after Mountjoy et al. (2009, 2014). Black lines are normal faults; “BSR” marks the location of a bottom simulating reflection, marking the base of gas hydrate stability, on this profile. The inset shows a zoom around the BSR. The dashed box on the interpreted seismic profile marks the exact location of this zoom extraction. The vertical exaggeration is ~ 7 times at 1,500 m/s. BSR = bottom-simulating reflection; TWT = two-way travel time.

Between 9 and 13.2 km along profile and below the MTDs, the reflections are dissected by the previously described normal faults (compare Figure 3). The normal faults cause small (< 0.019 -s TWT; 15 m) vertical displacements of the reflections. About 70% of the normal faults dip landward toward the NW (Figure 4). Some of the normal faults exhibit high-amplitude fault plane reflections. In the upward direction within the region where MTD1 is absent, most normal faults can be traced to MTD 2, the shallowest of the Tuaheni Landslide Complex deposits. The chaotic facies of the MTD and the rugged seafloor morphology inside the 3-D seismic volume complicate fault identification at shallow depths and at the seafloor (Figure 4).

3.3. Characteristics of the Normal Faults

We used the Symmetry I3D Energy seismic attribute and applied it to four horizons: the seafloor, the base of the most recent mass transport MTD 2, and clinoform surfaces A and B (Figure 5). Consequently, we are able to derive fault parameters at different stratigraphic levels. The fault parameters include spatial distribution, strike direction, true dip angles, dip direction, vertical displacement, and vertical extent of traceable fault planes. Our attribute analyses reveal sail line-induced seismic artifacts (Figure 5). As the sail lines strike at a different angle than the normal faults, they do not interfere with our analysis.

Clinoforms A and B display a wide network of linear anomalies in the Symmetry I3D Energy with coherent low attribute values, which indicate amplitude variations attributed to faults or noise (Figure 5). Because linear

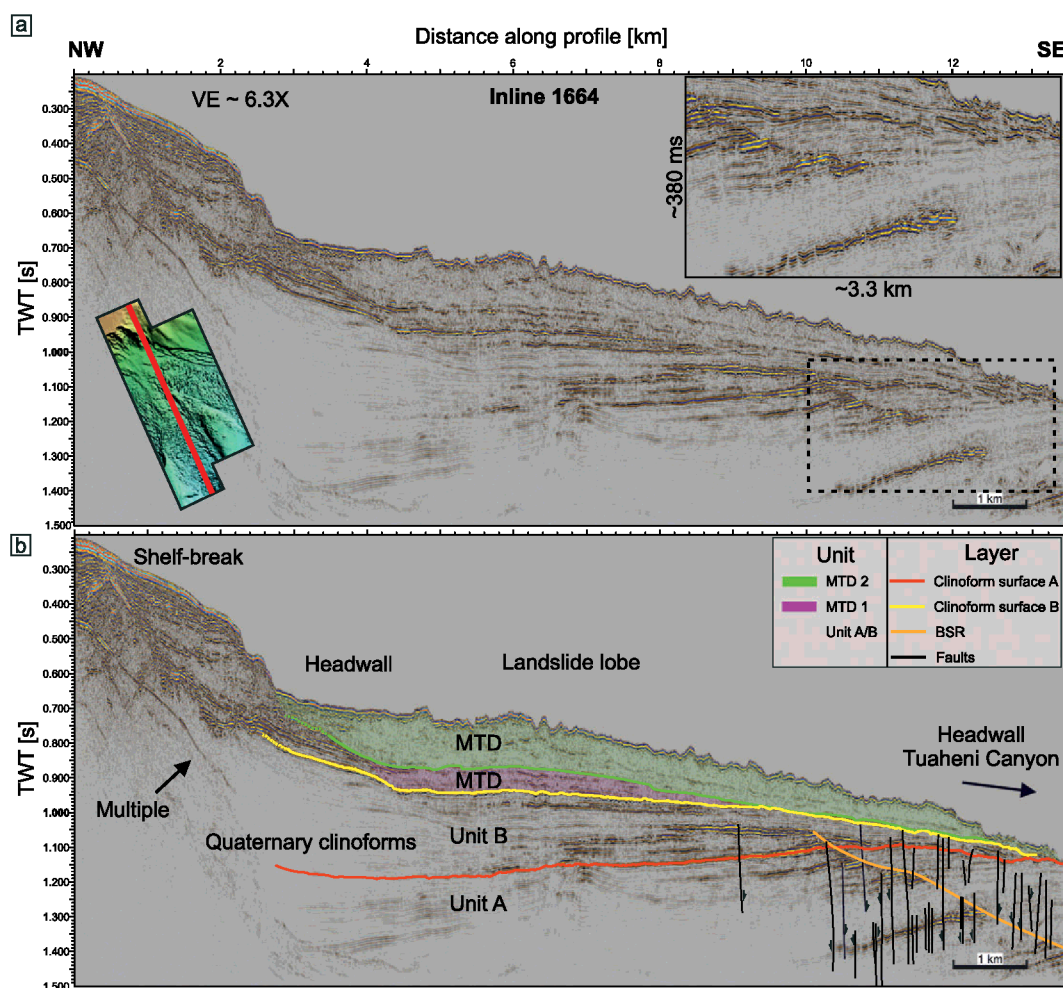


Figure 4. (a) Uninterpreted and (b) interpreted seismic reflection inline 1664 from the high-resolution 3-D seismic volume SCHLIP3D. The left inset in (a) shows the location of the profile (red line) within the extent of 3-D seismic coverage (note: the black box in Figure 1a shows the regional location of the 3-D seismic survey). The right inset in (a) shows a zoom of the normal faults (from the region enclosed by the dashed box). The vertical exaggeration is ~ 6.3 times at 1,500 m/s. SCHLIP3D = Submarine Clathrate Hydrate Landslide Imaging Project in 3-D; TWT = two-way travel time; MTD = mass transport deposit.

attribute anomalies can also be caused by noise in amplitude data, we cross-checked their locations with the locations of the low-displacement faults on vertical seismic displays (2-D profiles) between 10 and 15 km along profile and 1.2- to 1.5-s TWT (Figure 4). The comparison confirms that the linear attribute anomalies are all caused by vertical displacement along the faults. The faults exist within the 3-D seismic volume from the southwestern to the northeastern edge over an area of about 30 km².

The base of MTD 2 shows fewer linear attribute anomalies with predominantly north and northeastern strike directions (Figure 5). Cross-checking the seismic attributes with amplitude data on vertical displays confirms a decrease of traceable faults to this horizon (Figure 4). At the seafloor, no linear attribute anomalies with the characteristic azimuth angles are observed (Figure 5). We can conclude that either (a) the faults do not extend all the way to the seafloor or (b) surficial deformation fabrics of the landslide system have overprinted any structural signal from active faulting.

The vast majority of the normal faults is interconnected and forms a network with arcuate (in plan view) fault plane shapes (Figure 5). A minor group of faults is connected through small-scale fault triplets perpendicular to their planes (Figure 5). Fault triplets are three en echelon faults with fault planes that intersect / connect at depth. Throughout the whole fault network, fault planes in juxtaposition show rhombic-shaped subsided sections in between (Figure 5). The normal faults occur at high angles with 75% of all mapped faults dipping greater than 80°. In combination, these observations indicate that normal faulting may include a

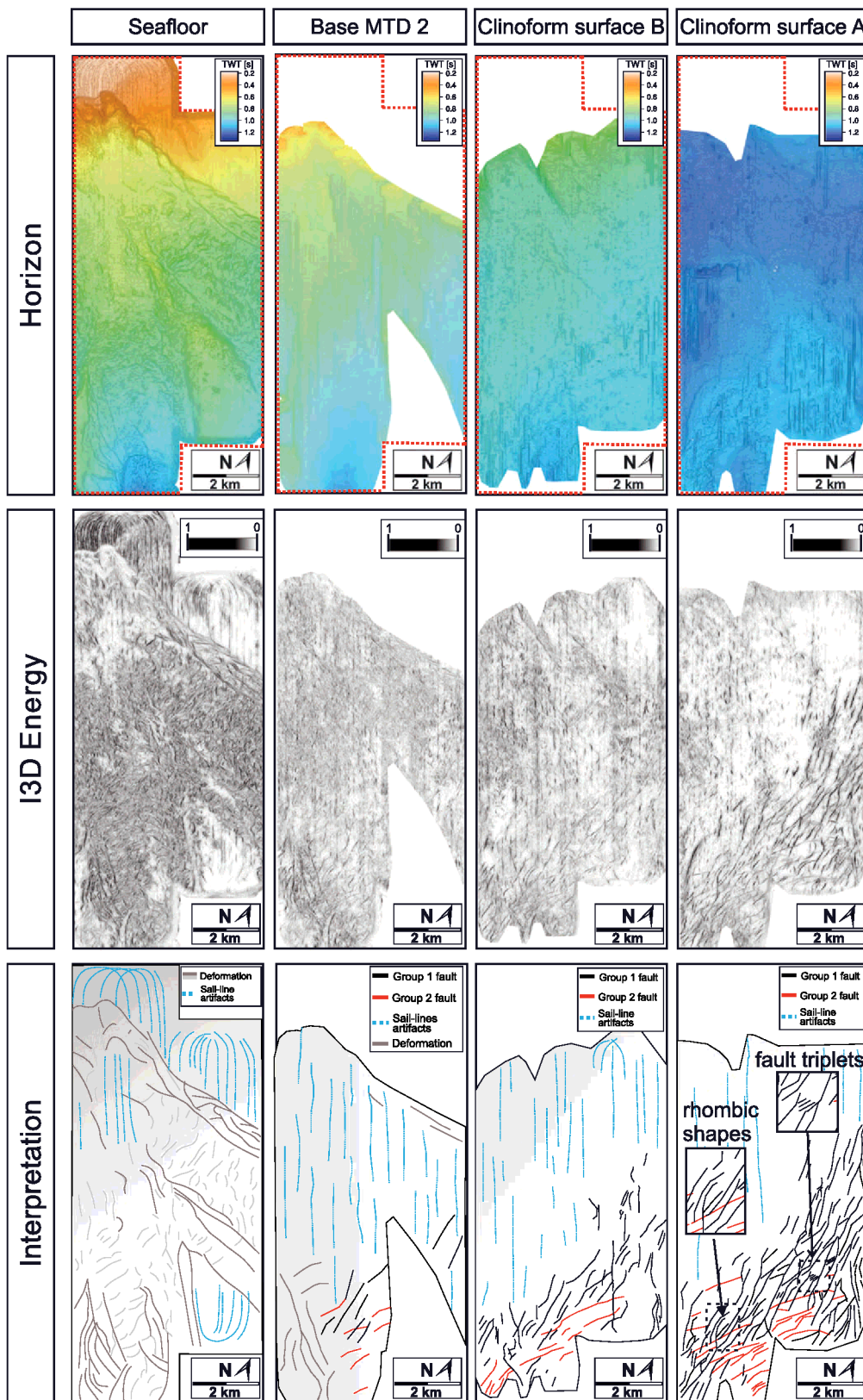


Figure 5. (top) This row shows seismic horizons at stratigraphic surfaces (surfaces as labeled in Figure 4b). The regional location of the seismic volume is shown in Figure 1a. (center) This row shows seismic horizon analysis with the I3D (Illuminator 3-D) Energy attribute. (bottom) Interpretation of seismic attribute maps on aforementioned horizons. MTD = mass transport deposit.

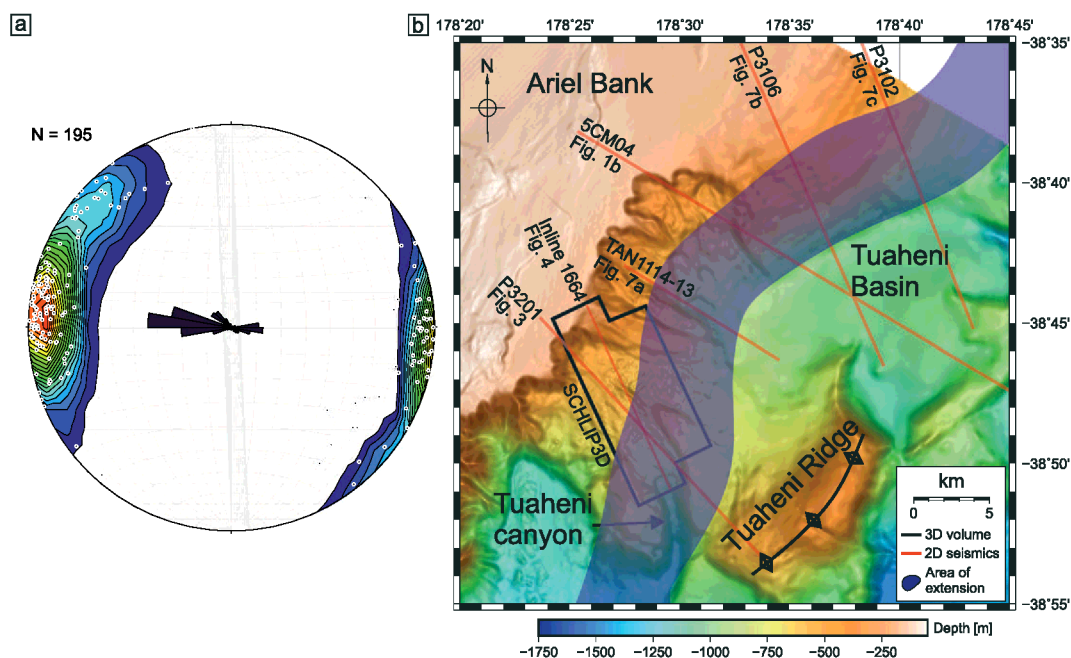


Figure 6. (a) Distribution of mapped normal faults on a stereographic projection (plotted with Stereonet software (Allmendinger et al., 2011; Cardozo & Allmendinger, 2013)). Rose diagram gives distribution of faults within a 10° range. The colored contour is an indicator for distribution over dip and azimuth. Two major strike directions are evident in the rose diagram: (40–60°) and (350–10°): The latter being parallel to the deformation front and other active faults on the lower trench slope (Figure 1). The majority of faults are dipping landward at very high angles (> 65°). (b) Bathymetric map showing locations of 2-D (red lines) and 3-D (black polygon) seismic data and the distribution of normal faults across the upper slope (semitransparent blue region). The normal faults are confined between the shelf break and the upper slope of Tuaheni Basin.

transtensional component, since transtensional movement is typically accommodated on multiple steeply dipping faults that intersect at depth (Woodcock & Fischer, 1986).

In total, we characterized 195 faults in terms of their spatial distribution, strike direction, dip angles, dip direction, vertical displacement, and vertical extent of traceable fault planes (Figure 6). The strike directions of the normal faults can be categorized into two groups. About 80% of the faults strike 350–15°, and ~10% show an azimuth of 40–60°. The remaining 10% of the normal faults lie outside of the two major strike directions (Figure 6). By extending the results from the 3-D data onto 2-D profiles, we observe a decrease in fault dip angle with decreasing distance from Tuaheni Ridge.

The decreasing seismic resolution of the 3-D seismic volume toward the acoustic basement limits the measurable vertical fault length to a maximum of 0.15-s TWT (~120 m at 1,600 m/s, Figure 4). Vertical displacements are in the range of 4–15 m (Figure 4) and derived horizontal displacements per unit length in the range of 0–3 m (Figure 2). The analysis of fault dip direction shows that 70% of all faults dip landward, 20% dip seaward, and 10% are near vertical (Figure 6).

3.4. Regional Extent of Normal Faulting

Upper-plate normal faults within the NE Hikurangi margin are not limited to the 3-D seismic volume but occur over a large area. Two-dimensional seismic profiles across the upper slope show widespread normal faulting within the upper 500 m of the seafloor (Figure 7). The presence of seafloor scarps overlying the seismically imaged fault planes (Figure 7) indicates that, if not masked by mass-transport deposits (like in the area of the SCHLIP3D data), extensional deformation continues to the seafloor. With our spatially limited 2-D seismic data, we are able to map normal faulting along the upper continental slope between 38°55'S to 38°35'S (Figure 6). In this area, the normal faults are abundant across the slope in between the shelf break and the upper-slope basins, confined to 500- to 1,000-m water depth. These latitudes, however, only represent the minimum spatial extent of upper-plate extension, and normal faulting may well continue farther along the margin.

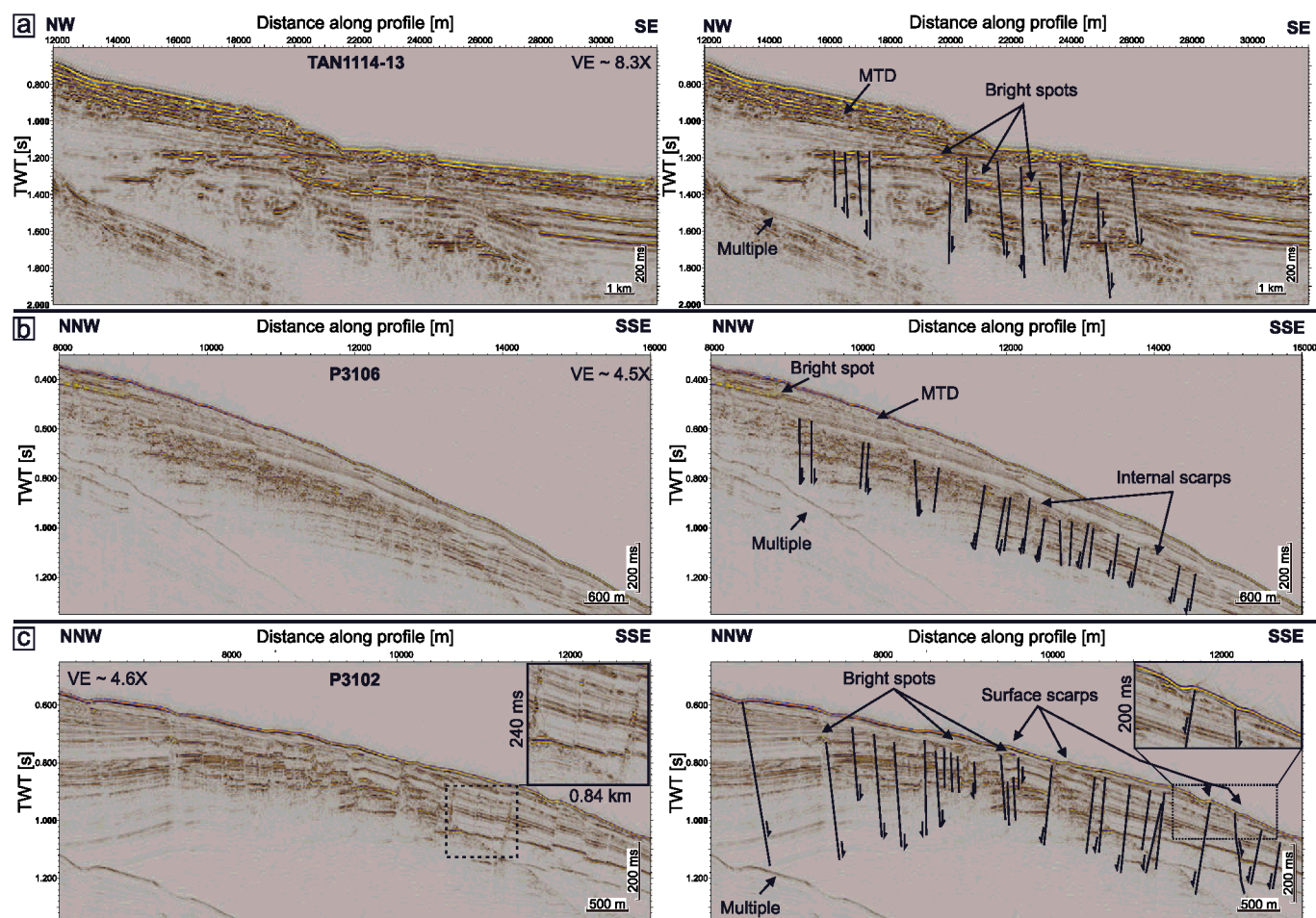


Figure 7. Uninterpreted and interpreted seismic profiles (a) TAN1114-13, (b) P3106, and (c) P3102 (locations on Figures 1a and 6b). (a) Seismic profile TAN1114-13 shows a mass transport deposit (MTD), normal faults, and bright spots associated with the normal faults indicating the presence of fluids inside pore space. The vertical exaggeration is 8.3 times at 1,500 m/s. (b) Seismic profile P3106 showing a MTD and bright spots indicating fluid flow inside the sedimentary succession (after Micallef et al., 2016). The abundant normal faults show vertical displacement resulting in internal scarps. These scarps are overprinted by downslope sedimentary processes. The vertical exaggeration is 4.5 times at 1,500 m/s. (c) Seismic profile P3102 showing prolonged normal faults with associated bright spots and high-amplitude reflection fault planes (inset uninterpreted profile). Many normal faults cut the seafloor and form scarps. The inset on the interpreted profile emphasizes these surface scarps that indicate that there is recent/active normal faulting across the marine forearc of Hikurangi margin. The vertical exaggeration is 4.6 times at 1,500 m/s. TWT = two-way travel time

4. Discussion

Geodetic measurements (Wallace et al., 2004, 2012), the analysis of regional seismicity (Reyners & McGinty, 1999), and structural investigations (Cashman & Kelsey, 1990) have provided evidence for upper-plate extension within the terrestrial parts of the Central Hikurangi and Raukumara tectonic blocks of the North Island (Figure 8). Our study area is located at the boundary between these two blocks, and we are able to extend the analysis of upper-plate extension into the marine forearc.

4.1. Decoupling and Gravitational Collapse of Shallow Strata

For other accretionary margins such as Cascadia and Nankai, upper-slope normal faulting has been suggested to result from decoupling of shallow strata from the underlying compressional wedge (Gulick et al., 2010; McNeill et al., 1997; Moore et al., 2013; Sacks et al., 2013). We compare the normal faults identified in our Hikurangi margin study area to the normal fault systems at Cascadia and Nankai.

Off Cascadia, listric normal faults occur in less than 1,000-m water depth, detach to a relatively shallow crustal décollement, and dip seaward with hundreds of meters vertical displacements (McNeill et al., 1997). Normal

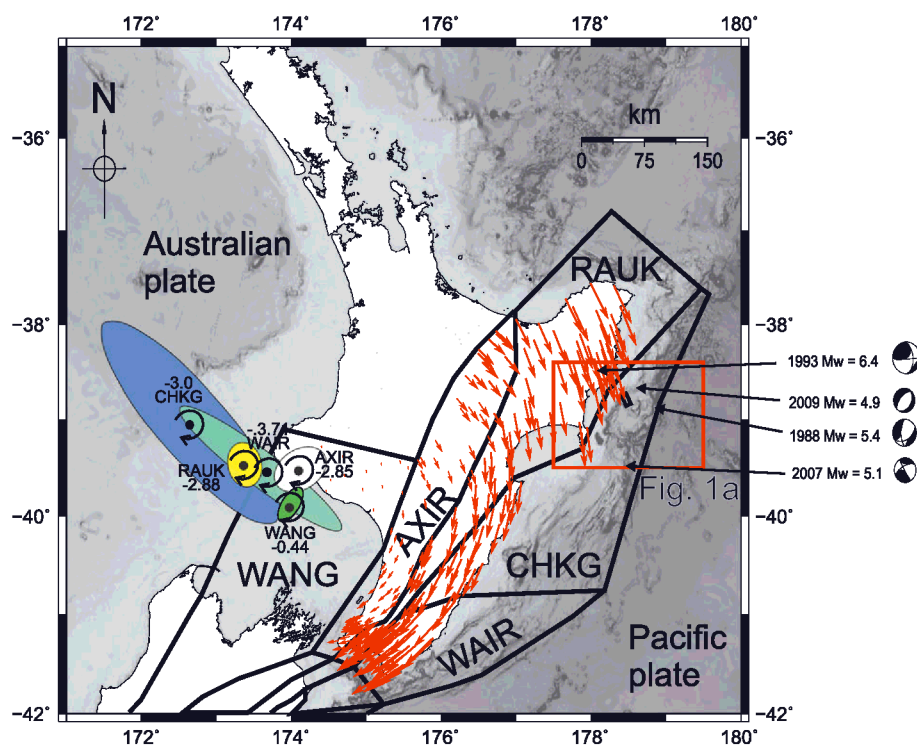


Figure 8. Bathymetric (GEBCO) map of the North Island and northwestern South Island of New Zealand with GPS velocity field (red arrows) and block model introduced by Wallace et al. (2004) with tectonic microblocks that rotate clockwise around nearby poles (modified after Nicol & Wallace, 2007; Wallace et al., 2004). All velocities are shown relative to the Australian Plate. Error ellipses are at 68% confidence level. The rotation rates are given in degree per Myr with negative values for clockwise rotation. WAIR = Wairarapa block; AXIR = axial ranges block; RAUK = Raukumara block; CHKG = Central Hikurangi block; WANG = Wanganui block. Red square marks the bounds of our survey area (Figure 1a). Focal mechanisms are taken from the global CMT catalog (Dziewonski et al., 1981; Ekström et al., 2012).

faults at Cascadia margin may be associated with contemporaneous gravity sliding on midcrustal layers or décollement surfaces (Buck & Sokoutis, 1994; Zoback et al., 1981) and suggest a decoupling of the shelf and upper slope from the subduction thrust (McNeill et al., 1997). Generally, the normal fault system, which we observe on this part of the Hikurangi margin, differs from what has been observed at the Cascadia margin offshore Grays Harbor, Washington, United States. We do not observe a predominantly seaward dip for the faults, nor the large offsets, nor a listric character and shallow detachment.

The normal fault system in Nankai resembles many characteristics of the normal faults we observe in this study. In the Kumano Basin, Nankai Trough (Japan), normal faults show high dip angles, preferred landward dip, distinct groups of strike, and many of the faults cut the seafloor indicating recent activity (Gulick et al., 2010; Moore et al., 2013; Sacks et al., 2013). There the normal faults have been mapped with a similar attribute-based seismic interpretation, and extension of the Kumano forearc basin is attributed to decoupling of shallow strata from the underlying thrust (Moore et al., 2013). Despite the structural similarities between the normal fault systems in the Hikurangi and the Nankai margins, there remain some arguments against a similar genetic origin. First, landward dipping thrust faulting in our study area continues to shallow strata (Figures 1a and 3). This contradicts a possible decoupling of the latter from the underlying compressional wedge (Mountjoy & Barnes, 2011). Second, the normal faults form at the lower boundary of the upper slope, in regions of shallow inclined seafloor (Figures 1a and 6). If these faults were an effect of compensatory movement due to uplift, we would expect them to occur predominantly in steeper areas farther downslope, where normal faults are absent (Figures 1b, 3, and 7). Such compensatory movement and subsequent extensional deformation have been observed at distinct anticlinal ridges farther south on the margin, where normal faults and fractures developed in response to flexural extension around the apex of folding (Barnes et al., 2010;

Wang et al., 2017). Third, the normal faults in our study area show a clear landward dipping preference and no change in dip angle with depth (see Figures 1b, 3, and 4).

In summary, the seismic data from Hikurangi do not reveal any midcrustal detachment, listric fault behavior, or large displacement normal faults. We therefore conclude that decoupling of shallow strata from the underlying compressional wedge and related gravitational collapse of the upper plate is an unlikely mechanism for upper-plate extension on the northern Hikurangi margin.

4.2. Extension as a Result of Uplift

Active faults on the onshore Raukumara Peninsula are predominantly extensional structures that are responding to rapid landscape uplift and are not thought to play a significant role in crustal deformation (Berryman et al., 2009). Active extension is also mapped onshore in Hawke's Bay to the south of our study area (Cashman & Kelsey, 1990). Uplift has been related to sediment underplating beneath the Raukumara range (Eberhart-Phillips & Chadwick, 2002; Walcott, 1987) and either margin tectonic deformation or underplating in the south. Bell et al. (2010) found a HRZ-2 in several multichannel seismic profiles beneath the offshore northern Hikurangi forearc. The location of this anomalous reflectivity results in an ambiguous interpretation of the plate interface thrust (Figures 1b and 9b). One possible interpretation of HRZ-2 is that it represents sedimentary material that is underplated at the base of the upper plate (Figure 9b). Pecher et al. (2014, 2017) invoke substantial uplift in the northern region of normal faulting as forming a pronounced double BSR at the base of gas hydrate stability. No clear indication of sediment underplating has been found for the offshore forearc.

A somewhat different driving mechanism for uplift may be the subduction of excess topography (Figure 9b). There is ample evidence that the subduction of seamounts or basement ridges increases the structural complexity of a margin (Bangs et al., 2006; Geersen et al., 2015; Gulick et al., 2004; Kodaira et al., 2000; Park et al., 2004; Ranero & von Huene, 2000; Wang & Bilek, 2011). Usually, the process of seamount subduction results in severe fracturing of the overriding plate above and around the subducting seamount (Dominguez et al., 1998; Wang & Bilek, 2011). The track of the subducting seamount is recorded in the deformation pattern of the upper plate (Dominguez et al., 1998). Above the seamount, arcuate thrust faults, subvertical fan-shaped fracture networks, and strike-slip faults develop which usually crosscut each other. In addition, normal faults, which show no consistent strike direction, form due to collapse of the upper plate in the wake of the subducting seamount (Dominguez et al., 1998; Wang & Bilek, 2011).

At multiple locations within the Hikurangi margin, subducting seamounts are known to have caused localized uplift, out of sequence faulting and large-scale mass failure (Barnes et al., 2010; Pedley et al., 2010). These deformation patterns are, for example, observed at the Poverty Bay indentation, which is located ~25-km southwest of our study area. Here seamount subduction initiated during the past ~ 2 Ma leads to a gravitational collapse of the upper plate in the wake of the seamount (Pedley et al., 2010; Wang & Bilek, 2011). In the area of our study, a subducting seamount is interpreted under the midslope area between 18 and 54 km along seismic line 05CM-04 (Figure 1b; Bell et al., 2010) which may lead to uplift and hence cause extension of the upper plate (Figure 9b). The documented normal fault system is, however, located between 450- and 1,200-m water depths on the landward side of the subducting seamount. It further shows a clear preference for landward dip, and the majority of faults have a margin parallel strike (Figures 4–7). As such, our structural observations do not completely agree with observed and modeled deformation patterns caused by subducting seamounts at accretionary margins elsewhere (Dominguez et al., 1998; Ranero & von Huene, 2000; Ruh et al., 2016). This does not rule out the possibility that seamount subduction induces regional uplift inducing extensional deformation at the upper slope. However, the structural discrepancies indicate that other processes that could also drive upper-plate extension may be active at the same time.

Regardless of a driving mechanism for uplift (underplating and seamount subduction are two possible mechanisms), a manifestation of upper-plate folding in the vicinity of the normal faults can be observed on Line 05CM-04, where subtle bending of upper-plate strata is seen (Figure 1b). As such, we consider flexural extension near the apex of folding (Figure 9b) as a mechanism that could lead to the extension in the areas where we have mapped the normal faults (Figure 6b). Flexural extension and normal faulting around the apex of folding is well known from other parts of the Hikurangi margin (Barnes et al., 2010; Wang et al., 2017), as well as on other convergent margins (e.g., López et al., 2010).

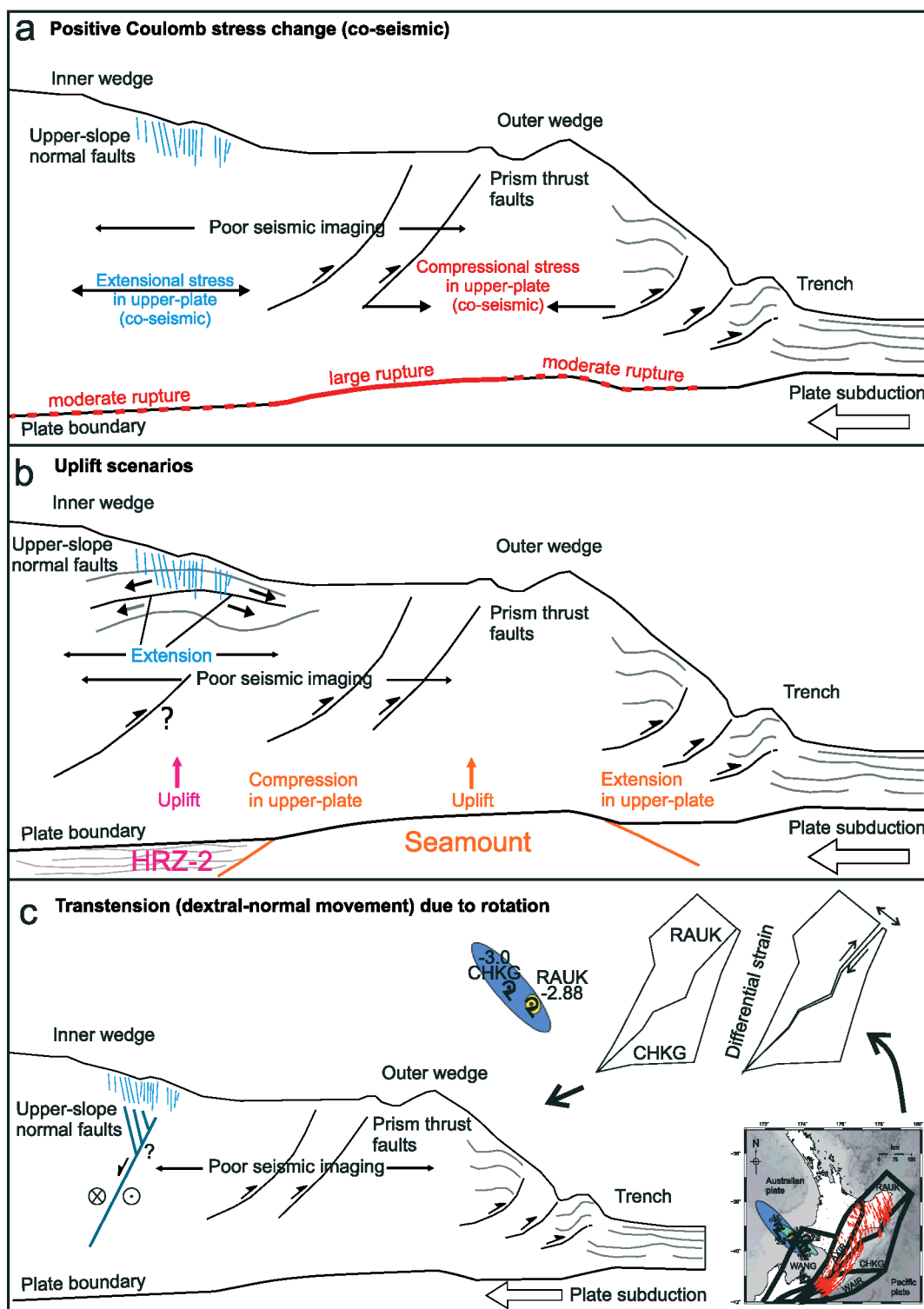


Figure 9. Conceptual models of the Hikurangi margin and mechanisms for marine forearc extension: (a) Positive Coulomb stress increase induced into the upper plate during the coseismic phase of earthquakes (after Aron et al., 2013; Fariás et al., 2011; Geersen et al., 2016; Toda et al., 2011). (b) Regional uplift due to underplating (magenta arrow; Bell et al., 2010; Cashman & Kelsey, 1990) or seamount subduction (orange arrow; after Dominguez et al., 1998; Wang & Bilek, 2011). Also shown is flexural extension around the apex of long-wavelength folding in the upper part of the wedge. (c) Transtension (dextral-normal movement) accommodated in the upper plate, induced into the marine forearc by residual extensional strain by differential clockwise rotation of Raukumara and Central Hikurangi microtectonic blocks around nearby poles (modified after Nicol & Wallace, 2007; Wallace et al., 2004). HRZ = high-amplitude reflectivity zone 2.

4.3. Extension as a Result of Positive Coulomb Stress Increase

The 2010 Chile (M_w 8.8) and 2011 Japan (M_w 9.0) earthquakes were accompanied by large-magnitude ($\sim M_w = 7.0$) extensional aftershocks that nucleated on upper-plate normal faults above the seismogenic zone (Fariás et al., 2011; Toda et al., 2011). In both cases, subsequent studies confirmed that the extensional aftershocks, which first took the scientific community by surprise, were related to the subduction process and the regional earthquake cycle (compare Figure 9a). For the 2010 Maule earthquake, different authors suggested that a positive Coulomb stress change induced into the upper plate by rupture of the underlying plate boundary-triggered normal faulting in some parts of the marine forearc (Figure 9a; Aron et al., 2013; Fariás et al., 2011; Geersen et al., 2016). The same process was likely responsible for upper-plate normal faulting in the wake of the 2011 Japan earthquake (Toda et al., 2011). In both cases, upper-plate normal faulting was possibly driven by dynamic weakening of the plate boundary, which moved the forearc into a critical extensional stress regime during the coseismic phase, likely further contributing to upper-plate normal faulting (Cubas, Avouac, Leroy, & Pons, 2013; Cubas, Avouac, Souloumiac, & Leroy, 2013).

To evaluate our mapped normal faults in the context of seismic rupture during a large megathrust earthquake, we need to consider the subduction interface in terms of fault behavior. The normal faults are located on the upper slope above a region of low interseismic coupling ($\phi < 0.5$) of the plate interface (Wallace et al., 2009). The region has hosted two moderate magnitude tsunami earthquakes ($M_w \sim 7.0$) in 1947 as well as a series of slow-slip events in recent years (Doser & Webb, 2003; Wallace et al., 2016). However, no large ($> M_w$ 8) plate boundary earthquake which may have caused permanent extensional deformation of the upper plate, as it happened during the 2010 Chile and 2011 Japan events, has yet been recorded in the area of the normal faults (Doser & Webb, 2003). While the potential for large megathrust earthquakes in the region remains an outstanding research question, our current knowledge on the seismotectonic setting makes it questionable whether the mapped pervasive extensional deformation of the upper plate solely relates to large plate boundary earthquakes.

4.4. Extension as a Result of Clockwise Rotation of the Hikurangi Forearc

Our analysis shows that aspects of the structural character of the normal fault system in the Hikurangi margin differ from forearc normal fault systems reported from other accretionary margins such as Nankai or Cascadia. In combination with differences in the large-scale tectonic setting of the upper plate (e.g., continuation of thrust faulting to shallow strata), we conclude that the origin of the normal faults in the Hikurangi margin may require a new explanation. Below, we consider whether stress and strain domains identified in geodetic modeling may contribute to normal faulting at the northeastern Hikurangi margin.

4.4.1. Tectonic Block Rotation as an Alternative Model to Explain Upper-Plate Extension

Oblique convergence, as it is the case in most active margins, usually results in strain partitioning within the forearc and/or the volcanic arc (Fitch, 1972; Teyssier et al., 1995). In some subduction zones, the oblique component is accommodated along prominent crustal-scale strike-slip faults, which extend parallel to the trench and the coastline over hundreds to thousands of kilometers. Prominent examples for such faults are the Liquiñe-Ofqui fault in Central and Southern Chile (Hervé, 1994) or the Mentawai Fault Zone off Sumatra (Diament et al., 1992). In other subduction settings, oblique convergence causes the development of individual tectonic blocks, which rotate around nearby poles (e.g., Cascadia, Marianas, Vanuatu, and Papua New Guinea; Calmant et al., 2003; Kato et al., 2003; McCaffrey et al., 2000; Wallace et al., 2004).

Off northeastern New Zealand, oblique convergence of the Pacific Plate in combination with an overall decrease in convergence rate toward the south results in clockwise rotation of North Island crustal blocks around poles lying to the west of the North Island (Figure 8; Mumme et al., 1989; Walcott, 1984; Wallace et al., 2004). Geodetic measurements, earthquake slip vectors, and geological fault slip rates have been used to estimate the angular velocities of the tectonic blocks and the degree of coupling along the faults, which separate the different blocks (Wallace et al., 2004). In some parts of the marine forearc, block rotation is expected to result in extensional differential stresses. Although most of the extensional budget resulting from the rotation can be explained by slip on normal faults within the Taupo volcanic zone, minor positive residual strain ($1\text{--}35 \times 10^{-9}$) is calculated for the eastern North Island forearc blocks (Wallace et al., 2004). For scale, a strain rate of 20×10^{-9} for the Wairarapa block (50-km wide) causes 1-mm/year differential slip rate. Wallace et al. (2004) suggest that the residual strain might be released by slip on previously unrecognized extensional

faults along the block boundaries. However, widespread upper-plate extension had not been observed previously for the northeastern and central marine forearc of the Hikurangi margin.

The upper-plate normal faults we have identified in the study area beneath the upper continental slope may represent a fault system that accommodates such residual strain. From their location and spatial distribution, the normal faults would accommodate extensional stresses between the Raukumara and the Central Hikurangi blocks (Figures 8 and 9c).

4.4.2. Application to the Northeastern Hikurangi Margin

Mountjoy et al. (2009) describe the shallow sedimentary succession in the study area as Quaternary low-stand clinoforms with Holocene sediments above (Figures 1b, 3, and 4). Profile 05CM04 (Figure 1b) suggests that the normal faults are confined to this section. Assuming a maximum age for the quaternary clinoforms of 0.4 Ma or younger (Mountjoy & Barnes, 2011) in combination with the minor positive residual strain of $1\text{--}35 \times 10^{-9}$ (Wallace et al., 2004), the maximum dilatation of the crustal block would cumulate to ~ 400 m of extension. The 195 faults within the 3-D seismic volume cumulate to a total horizontal displacement of approximately 120 m. However, the 3-D seismic volume does not cover the full spatial extent of the normal faults in the across-slope direction. Based on 2-D seismic line P3201, we estimate that our 3-D seismic volume covers approximately two thirds of the whole fault network and uses this line (Line P3201) to extrapolate the total horizontal displacement. We estimate that the fault network could account for about 180 m of total horizontal displacement. The normal fault network thus covers bulk extension within the same order of magnitude as proposed by the modeled block rotation (Wallace et al., 2004).

In 2009, an extensional earthquake (M_w 4.9) with a minor strike-slip component took place within the upper plate in the area of this study (Figures 1a and 8). The en echelon normal faults we image in this study enclose rhombic-shaped subsided areas, show high dip angles ($75^\circ > 80^\circ$), and are interconnected by small-scale fault triplets (Figures 5 and 6). These observations indicate duplex structures in the subsurface and hence a transtensional (dextral-normal) character of the fault network (Woodcock & Fischer, 1986). Together with the 2009 earthquake, this lends support to the hypothesis that the differential stresses between the Central Hikurangi and the Raukumara tectonic blocks may have contributed to the development of normal faults in the marine forearc of the northeastern Hikurangi margin (Figures 8 and 9c).

These indications are consistent with observations in Crete, Greece, where transtension in the Hellenic forearc forms sinistral-normal faults with distinct azimuth groups because of rotation (Ten Veen & Kleinspehn, 2003). Similar to our indications for transtension (though dextral in our case), the sinistral-normal deformation in Crete is inferred from en echelon rhombic depressions and ridges (Huchon et al., 1982; Huguenot et al., 2001). This proposed model (Figure 9c) agrees with local observations farther south within the Central Hikurangi block, where shear structures form in combination with protothrusts and extensional faults at Omakere Ridge (Plaza-Faverola et al., 2014).

5. Conclusions and Outlook

Our study documents extension within the marine forearc of the Hikurangi margin based on 2-D and 3-D seismic data. We map and analyze normal faults with low vertical displacements over an along-margin distance of at least 50 km. These faults occur between the shelf break and the upper-slope basins and are confined to 500- to 1,000-m water depth. We draw the following main conclusions:

1. The normal faults at the upper slope of the Hikurangi margin show two major strike directions, primarily landward dip, and steep fault angles. Where MTDs are absent, seafloor scarps indicate recent fault activity. The normal faults are interconnected, for example, by small-scale fault triplets, enclose rhombic-shaped subsided sections, and the majority dips at angles $>80^\circ$. These observations suggest transtensional deformation.
2. Mechanisms that may have contributed to the development of the normal faults in the Hikurangi margin include uplift and gravitational collapse and/or flexural bending of the upper plate and residual extensional strain, which is induced into the marine forearc by rotation of tectonic blocks around nearby poles.

The block rotation model agrees with the transtensional character of the normal faults. However, the limited spatial (and depth) extent of our seismic data does not allow us to ultimately resolve the dominant tectonic process behind the generation of the normal faults. As in any complex geologic system, the interplay of

different processes may be responsible for causing marine forearc extension in the northeastern Hikurangi margin.

Our work adds another piece of evidence that normal faults play an important role in the seismotectonic evolution of accretionary margins. However, a better understanding of the mechanisms that cause upper-plate extension in the different place remains a research challenge. Large-scale 3-D seismic experiments and scientific drilling may provide critical data to further investigate the driving mechanisms behind forearc normal faulting.

Acknowledgments

The collection and processing of the P-Cable 3-D volume and 2-D data were jointly funded by the New Zealand Ministry for Business Innovation and Employment (MBIE), NIWA, GNS Science Core funding, and the Deutsche Forschungsgemeinschaft (DFG-grant Bl 404/7 | KR 2222/18). Jacob Geersen was funded by a grant (CP1404) of the Cluster of Excellence 80 “The Future Ocean”. The Future Ocean is funded within the framework of the Excellence Initiative by the Deutsche Forschungsgemeinschaft (DFG) on behalf of the German federal and state governments. We thank the officers and crew of RV *Tangaroa* and all the shipboard participants who made the data collection possible. Line TAN114-13 was collected on voyage TAN1114 led by Philip Barnes and funded by MBIE through OS2020 and NIWA and GNS Science SSIF funding. Stuart Henrys processed the TAN1114 seismic data onboard. Line 05CM-04 was collected by Crown Minerals for the New Zealand Government (<https://www.nzpam.govt.nz/maps-geoscience/>). Access to the bathymetric and seismic data is through NIWA marine data repository (<https://marinedata.niwa.co.nz/project-map-sam/>). The corresponding author would like to thank Christian Berndt for his support during the process of writing this manuscript. We thank IHS for providing the Kingdom software through their University Grant Program. We thank Gregory F. Moore and one anonymous reviewer for their careful reviews that helped us to clarify different aspects of this study.

References

- Alexander, C. R., Walsh, J. P., & Orpin, A. R. (2010). Modern sediment dispersal and accumulation on the outer poverty continental margin. *Marine Geology*, 270(1–4), 213–226. <https://doi.org/10.1016/j.margeo.2009.10.015>
- Allmendinger, R. W., Cardozo, N., & Fisher, D. M. (2011). *Structural geology algorithms: Vectors and tensors*. Cambridge: Cambridge University Press. <https://doi.org/10.1017/CBO9780511920202>
- Aron, F., Allmendinger, R. W., Cembrano, J., González, G., & Yáñez, G. (2013). Permanent fore-arc extension and seismic segmentation: Insights from the 2010 Maule earthquake, Chile. *Journal of Geophysical Research: Solid Earth*, 118, 724–739. <https://doi.org/10.1029/2012JB009339>
- Asano, Y., Saito, T., Ito, Y., Shiomi, K., Hirose, H., Matsumoto, T., et al. (2011). Spatial distribution and focal mechanisms of aftershocks of the 2011 off the Pacific coast of Tohoku Earthquake. *Earth, Planets and Space*, 63(7), 29.
- Bahorich, M., & Farmer, S. (1995). 3-D seismic discontinuity for faults and stratigraphic features: The coherence cube. *The Leading Edge*, 14(10), 1053–1058. <https://doi.org/10.1190/1.1437077>
- Bangs, N. L., Gulick, S. P., & Shipley, T. H. (2006). Seamount subduction erosion in the Nankai Trough and its potential impact on the seismogenic zone. *Geology*, 34(8), 701–704. <https://doi.org/10.1130/G22451.1>
- Barker, D. H., Sutherland, R., Henrys, S., & Bannister, S. (2009). Geometry of the Hikurangi subduction thrust and upper plate, North Island, New Zealand. *Geochimistry, Geophysics, Geosystems*, 10, Q02007. <https://doi.org/10.1029/2008GC002153>
- Barnes, P. M., Cheung, K. C., Smits, A. P., Almagor, G., Read, S. A., Barker, P. R., & Froggatt, P. (1991). Geotechnical analysis of the kidnappers slide, upper continental slope, New Zealand. *Marine Georesources & Geotechnology*, 10(1–2), 159–188. <https://doi.org/10.1080/10641199109379888>
- Barnes, P. M., Lamarche, G., Bialas, J., Henrys, S., Pecher, I., Netzeband, G. L., et al. (2010). Tectonic and geological framework for gas hydrates and cold seeps on the Hikurangi subduction margin, New Zealand. *Marine Geology*, 272(1–4), 26–48. <https://doi.org/10.1016/j.margeo.2009.03.012>
- Barnes, P. M., Nicol, A., & Harrison, T. (2002). Late Cenozoic evolution and earthquake potential of an active listric thrust complex above the Hikurangi subduction zone, New Zealand. *Geological Society of America Bulletin*, 114(11), 1379–1405. [https://doi.org/10.1130/0016-7606\(2002\)114<1379:LCEAE>2.0.CO;2](https://doi.org/10.1130/0016-7606(2002)114<1379:LCEAE>2.0.CO;2)
- Barnes, P., Mountjoy, J. J., Wilcox, S., Mitchell, S., Pallentin, A., Amyes, D., et al. (2011). National Institute of Water and Atmospheric Research (NIWA) Voyage Report, Ocean 2020 Northern Hikurangi Margin Geohazards, RV *Tangaroa* Rep. Tan1114, NIWA, Wellington, New Zealand.
- Beanland, S., & Haines, J. (1998). The kinematics of active deformation in the North Island, New Zealand, determined from geological strain rates. *New Zealand Journal of Geology and Geophysics*, 41(4), 311–323. <https://doi.org/10.1080/00288306.1998.9514813>
- Beavan, J., Tregoning, P., Bevis, M., Kato, T., & Meertens, C. (2002). Motion and rigidity of the Pacific Plate and implications for plate boundary deformation. *Journal of Geophysical Research*, 107(B10), 2261. <https://doi.org/10.1029/2001JB000282>
- Bell, R., Holden, C., Power, W., Wang, X., & Downes, G. (2014). Hikurangi margin tsunami earthquake generated by slow seismic rupture over a subducted seamount. *Earth and Planetary Science Letters*, 397, 1–9. <https://doi.org/10.1016/j.epsl.2014.04.005>
- Bell, R., Sutherland, R., Barker, D. H., Henrys, S., Bannister, S., Wallace, L., & Beavan, J. (2010). Seismic reflection character of the Hikurangi subduction interface, New Zealand, in the region of repeated Gisborne slow slip events. *Geophysical Journal International*, 180(1), 34–48. <https://doi.org/10.1111/j.1365-246X.2009.04401.x>
- Berryman, K., Marden, M., Palmer, A., & Litchfield, N. (2009). Holocene rupture of the Repongaere Fault, Gisborne: Implications for Raukumara Peninsula deformation and impact on the Waipaoa Sedimentary System. *New Zealand Journal of Geology and Geophysics*, 52(4), 335–347. <https://doi.org/10.1080/00288306.2009.9518462>
- Berryman, K. R., Ota, Y., & Hull, A. G. (1989). Holocene paleoseismicity in the fold and thrust belt of the Hikurangi subduction zone, eastern North Island, New Zealand. *Tectonophysics*, 163(3–4), 185–195. [https://doi.org/10.1016/0040-1951\(89\)90256-4](https://doi.org/10.1016/0040-1951(89)90256-4)
- Buck, W. R., & Sokoutis, D. (1994). Analogue model of gravitational collapse and surface extension during continental convergence. *Nature*, 369(6483), 737–740. <https://doi.org/10.1038/369737a0>
- Calmant, S., Pelletier, B., Lebellegard, P., Bevis, M., Taylor, F. W., & Phillips, D. A. (2003). New insights on the tectonics along the New Hebrides subduction zone based on GPS results. *Journal of Geophysical Research*, 108(B6), 2319. <https://doi.org/10.1029/2001JB000644>
- Cardozo, N., & Allmendinger, R. W. (2013). Spherical projections with OSXStereonet. *Computers & Geosciences*, 51, 193–205. <https://doi.org/10.1016/j.cageo.2012.07.021>
- Cashman, S. M., & Kelsey, H. M. (1990). Forearc uplift and extension, southern Hawke’s Bay, New Zealand: Mid-Pleistocene to present. *Tectonics*, 9(1), 23–44. <https://doi.org/10.1029/TC009i001p00023>
- Catuneanu, O., Abreu, V., Bhattacharya, J. P., Blum, M. D., Dalrymple, R. W., Eriksson, P. G., et al. (2009). Towards the standardization of sequence stratigraphy. *Earth-Science Reviews*, 92(1–2), 1–33. <https://doi.org/10.1016/j.earscirev.2008.10.003>
- Conly, G. (1980). *The shock of 31: The Hawke’s Bay earthquake*. Wellington: A.H. and A.W. Reed Ltd.
- Cubas, N., Avouac, J. P., Leroy, Y. M., & Pons, A. (2013). Low friction along the high slip patch of the 2011 Mw 9.0 Tohoku-Oki earthquake required from the wedge structure and extensional splay faults. *Geophysical Research Letters*, 40, 4231–4237. <https://doi.org/10.1002/grl.50682>
- Cubas, N., Avouac, J. P., Souloumiac, P., & Leroy, Y. (2013). Megathrust friction determined from mechanical analysis of the forearc in the Maule earthquake area. *Earth and Planetary Science Letters*, 381, 92–103. <https://doi.org/10.1016/j.epsl.2013.07.037>
- Davy, B., & Wood, R. (1994). Gravity and magnetic modelling of the Hikurangi Plateau. *Marine Geology*, 118(1–2), 139–151. [https://doi.org/10.1016/0025-3227\(94\)90117-1](https://doi.org/10.1016/0025-3227(94)90117-1)

- De Lange, W. P., & Healy, T. R. (1986). New Zealand tsunamis 1840–1982. *New Zealand Journal of Geology and Geophysics*, 29(1), 115–134. <https://doi.org/10.1080/00288306.1986.10427527>
- Diament, M., Harjono, H., Karta, K., Deplus, C., Dahrin, D., Zen, M. T., et al. (1992). Mentawai fault zone off Sumatra: A new key to the geodynamics of western Indonesia. *Geology*, 20(3), 259–262. [https://doi.org/10.1130/0091-7613\(1992\)020<0259:MFZOSA>2.3.CO;2](https://doi.org/10.1130/0091-7613(1992)020<0259:MFZOSA>2.3.CO;2)
- Dominguez, S., Lallemand, S. E., Malavieille, J., & von Huene, R. (1998). Upper plate deformation associated with seamount subduction. *Tectonophysics*, 293(3–4), 207–224. [https://doi.org/10.1016/S0040-1951\(98\)00086-9](https://doi.org/10.1016/S0040-1951(98)00086-9)
- Doser, D. I., & Webb, T. H. (2003). Source parameters of large historical (1917–1961) earthquakes, North Island, New Zealand. *Geophysical Journal International*, 152(3), 795–832. <https://doi.org/10.1046/j.1365-246X.2003.01895.x>
- Dziewonski, A. M., Chou, T. A., & Woodhouse, J. H. (1981). Determination of earthquake source parameters from waveform data for studies of global and regional seismicity. *Journal of Geophysical Research*, 86, 2825–2852. <https://doi.org/10.1029/JB086iB04p02825>
- Eberhart-Phillips, D., & Chadwick, M. (2002). Three-dimensional attenuation model of the shallow Hikurangi subduction zone in the Raukumara Peninsula, New Zealand. *Journal of Geophysical Research*, 107(B2), 2033. <https://doi.org/10.1029/2000JB000046>
- Ekström, G., Nettles, M., & Dziewoński, A. M. (2012). The global CMT project 2004–2010: Centroid-moment tensors for 13,017 earthquakes. *Physics of the Earth and Planetary Interiors*, 200, 1–9.
- Fariás, M., Comte, D., Roecker, S., Carrizo, D., & Pardo, M. (2011). Crustal extensional faulting triggered by the 2010 Chilean earthquake: The Pichilemu Seismic Sequence. *Tectonics*, 30, TC6010. <https://doi.org/10.1029/2011TC002888>
- Field, B. D., & Uruski, C. I. (1997). *Cretaceous-Cenozoic geology and petroleum systems of the East Coast region, New Zealand* (Vol. 1). Lower Hutt, New Zealand: Institute of Geological and Nuclear Sciences.
- Fitch, T. J. (1972). Plate convergence, transcurrent faults, and internal deformation adjacent to Southeast Asia and the western Pacific. *Journal of Geophysical Research*, 77, 4432–4460. <https://doi.org/10.1029/JB077i023p04432>
- Fraser, R. J. (1998). Historical tsunami database for New Zealand (Doctoral dissertation, Univ. of Waikato).
- Geersen, J., Behrmann, J. H., Völker, D., Krastel, S., Ranero, C. R., Diaz-Naveas, J., & Weinrebe, W. (2011). Active tectonics of the South Chilean marine fore arc (35 S–40 S). *Tectonics*, 30, TC3006. <https://doi.org/10.1029/2010TC002777>
- Geersen, J., Ranero, C. R., Barckhausen, U., & Reichert, C. (2015). Subducting seamounts control interplate coupling and seismic rupture in the 2014 Iquique earthquake area. *Nature Communications*, 6(1), 8267. <https://doi.org/10.1038/ncomms9267>
- Geersen, J., Scholz, F., Linke, P., Schmidt, M., Lange, D., Behrmann, J. H., et al. (2016). Fault zone controlled seafloor methane seepage in the rupture area of the 2010 Maule earthquake, Central Chile. *Geochemistry, Geophysics, Geosystems*, 17, 4802–4813. <https://doi.org/10.1002/2016GC006498>
- Grando, G., & McClay, K. (2007). Morphotectonics domains and structural styles in the Makran accretionary prism, offshore Iran. *Sedimentary Geology*, 196(1–4), 157–179. <https://doi.org/10.1016/j.sedgeo.2006.05.030>
- Gulick, S. P., Bangs, N. L., Moore, G. F., Ashi, J., Martin, K. M., Sawyer, D. S., et al. (2010). Rapid forearc basin uplift and megasplay fault development from 3D seismic images of Nankai Margin off Kii Peninsula, Japan. *Earth and Planetary Science Letters*, 300(1–2), 55–62. <https://doi.org/10.1016/j.epsl.2010.09.034>
- Gulick, S. P. S., Bangs, N. L. B., Shipley, T. H., Nakamura, Y., Moore, G., & Kuramoto, S. (2004). Three-dimensional architecture of the Nankai accretionary prism's imbricate thrust zone off Cape Muroto, Japan: Prism reconstruction via en echelon thrust propagation. *Journal of Geophysical Research*, 109, B02105. <https://doi.org/10.1029/2003JB002654>
- Hervé, F. (1994). The Southern Andes between 39 and 44 S latitude: The geological signature of a transpressive tectonic regime related to a magmatic arc. In *Tectonics of the Southern Central Andes* (pp. 243–248). Berlin: Springer.
- Huchon, P., Lybéris, N., Angelier, J., Le Pichon, X., & Renard, V. (1982). Tectonics of the Hellenic Trench: A synthesis of sea-beam and submersible observations. *Tectonophysics*, 86(1–3), 69–112.
- Huguenot, C., Mascle, J., Chaumillon, E., Woodside, J. M., Benkhelil, J., Kopf, A., & Volkonskaia, A. (2001). Deformational styles of the eastern Mediterranean Ridge and surroundings from combined swath mapping and seismic reflection profiling. *Tectonophysics*, 343(1–2), 21–47. [https://doi.org/10.1016/S0040-1951\(01\)00185-8](https://doi.org/10.1016/S0040-1951(01)00185-8)
- Ide, S., Baltay, A., & Beroza, G. C. (2011). Shallow dynamic overshoot and energetic deep rupture in the 2011 Mw 9.0 Tohoku-Oki earthquake. *Science*, 332(6036), 1426–1429. <https://doi.org/10.1126/science.1207020>
- Kato, T., Beavan, J., Matsushima, T., Kotake, Y., Camacho, J. T., & Nakao, S. (2003). Geodetic evidence of back-arc spreading in the Mariana trough. *Geophysical Research Letters*, 30(12), 1625. <https://doi.org/10.1029/2002GL016757>
- Kodaira, S., Takahashi, N., Nakanishi, A., Miura, S., & Kaneda, Y. (2000). Subducted seamount imaged in the rupture zone of the 1946 Nankaido earthquake. *Science*, 289(5476), 104–106. <https://doi.org/10.1126/science.289.5476.104>
- Kukowski, N., Greinert, J., & Henrys, S. (2010). Morphometric and critical taper analysis of the Rock Garden region, Hikurangi Margin, New Zealand: Implications for slope stability and potential tsunami generation. *Marine Geology*, 272(1–4), 141–153. <https://doi.org/10.1016/j.margeo.2009.06.004>
- López, C., Spence, G., Hyndman, R., & Kelley, D. (2010). Frontal ridge slope failure at the northern Cascadia margin: Margin-normal fault and gas hydrate control. *Geology*, 38(11), 967–970. <https://doi.org/10.1130/G31136.1>
- Masson, D. G., Parson, L. M., Milsom, J., Nichols, G., Sikumbang, N., Dwiyanto, B., & Kallagher, H. (1990). Subduction of seamounts at the Java Trench: A view with long-range sidescan sonar. *Tectonophysics*, 185(1–2), 51–65. [https://doi.org/10.1016/0040-1951\(90\)90404-V](https://doi.org/10.1016/0040-1951(90)90404-V)
- Mazengarb, C. (1984). The Fernside Fault: An active normal fault, Raukumara Peninsula, New Zealand. *New Zealand Geological Survey Record*, 3, 98–103.
- McCaffrey, R. (2002). Crustal block rotations and plate coupling. In *Plate boundary zones* (pp. 101–122). Washington, DC: American Geophysical Union.
- McCaffrey, R., Long, M. D., Goldfinger, C., Zwick, P. C., Nabelek, J. L., Johnson, C. K., & Smith, C. (2000). Rotation and plate locking at the southern Cascadia subduction zone. *Geophysical Research Letters*, 27, 3117–3120. <https://doi.org/10.1029/2000GL011768>
- McClusky, S. C., Bjornstad, S. C., Hager, B. H., King, R. W., Meade, B. J., Miller, M. M., et al. (2001). Present day kinematics of the eastern California shear zone from a geodetically constrained block model. *Geophysical Research Letters*, 28, 3369–3372. <https://doi.org/10.1029/2001GL013091>
- McNeill, L. C., Piper, K. A., Goldfinger, C., Kulm, L. D., & Yeats, R. S. (1997). Listric normal faulting on the Cascadia continental margin. *Journal of Geophysical Research*, 102, 12,123–12,138. <https://doi.org/10.1029/97JB00728>
- Micallef, A., Mountjoy, J. J., Krastel, S., Crutchley, G., & Koch, S. (2016). Shallow gas and the development of a weak layer in submarine spreading, Hikurangi margin (New Zealand). In *Submarine Mass Movements and their Consequences* (pp. 419–426). Wellington, New Zealand: Springer international Publishing.
- Moore, G. F., Boston, B. B., Sacks, A. F., & Saffer, D. M. (2013). Analysis of normal fault populations in the Kumano Forearc Basin, Nankai Trough, Japan: 1. Multiple orientations and generations of faults from 3-D coherency mapping. *Geochemistry, Geophysics, Geosystems*, 14, 1989–2002. <https://doi.org/10.1002/ggge.20119>

- Mountjoy, J. J., & Barnes, P. M. (2011). Active upper plate thrust faulting in regions of low plate interface coupling, repeated slow slip events, and coastal uplift: Example from the Hikurangi Margin, New Zealand. *Geochemistry, Geophysics, Geosystems*, 12, Q01005. <https://doi.org/10.1029/2010GC003326>
- Mountjoy, J. J., McKean, J., Barnes, P. M., & Pettinga, J. R. (2009). Terrestrial-style slow-moving earthflow kinematics in a submarine landslide complex. *Marine Geology*, 267(3-4), 114–127. <https://doi.org/10.1016/j.margeo.2009.09.007>
- Mountjoy, J. J., Pecher, I., Henriys, S., Crutchley, G., Barnes, P. M., & Plaza-Faverola, A. (2014). Shallow methane hydrate system controls ongoing, downslope sediment transport in a low-velocity active submarine landslide complex, Hikurangi Margin, New Zealand. *Geochemistry, Geophysics, Geosystems*, 15, 4137–4156. <https://doi.org/10.1002/2014GC005379>
- Mumme, T. C., Lamb, S. H., & Walcott, R. I. (1989). The Raukumara paleomagnetic domain: Constraints on the tectonic rotation of the east coast, North Island, New Zealand, from paleomagnetic data. *New Zealand Journal of Geology and Geophysics*, 32(3), 317–326. <https://doi.org/10.1080/00288306.1989.10425711>
- Neves, F. A., Zahrani, M. S., & Brekmp, S. W. (2004). Detection of potential fractures and small faults using seismic attributes. *The Leading Edge*, 23(9), 903–906. <https://doi.org/10.1190/1.1803500>
- Nicol, A., Mazengarb, C., Chanier, F., Rait, G., Uruski, C., & Wallace, L. (2007). Tectonic evolution of the active Hikurangi subduction margin, New Zealand, since the Oligocene. *Tectonics*, 26, TC4002. <https://doi.org/10.1029/2006TC002090>
- Nicol, A., & Wallace, L. M. (2007). Temporal stability of deformation rates: Comparison of geological and geodetic observations, Hikurangi subduction margin, New Zealand. *Earth and Planetary Science Letters*, 258(3-4), 397–413. <https://doi.org/10.1016/j.epsl.2007.03.039>
- Ota, Y., & Yamaguchi, M. (2004). Holocene coastal uplift in the western Pacific Rim in the context of late Quaternary uplift. *Quaternary International*, 120(1), 105–117. <https://doi.org/10.1016/j.quaint.2004.01.010>
- Park, J. O., Moore, G. F., Tsuru, T., Kodaira, S., & Kaneda, Y. (2004). A subducted oceanic ridge influencing the Nankai megathrust earthquake rupture. *Earth and Planetary Science Letters*, 217(1-2), 77–84. [https://doi.org/10.1016/S0012-821X\(03\)00553-3](https://doi.org/10.1016/S0012-821X(03)00553-3)
- Pecher, I., Crutchley, G., Mountjoy, J., Gorman, A., Fraser, D., & Henriys, S. (2014). Double BSRs on the Hikurangi Margin, New Zealand—Possible implications for gas hydrate stability and composition. In *8th International Conference on Gas Hydrates*.
- Pecher, I. A., Villinger, H., Kaul, N., Crutchley, G. J., Mountjoy, J. J., Huhn, K., et al. (2017). A fluid pulse on the Hikurangi subduction margin: Evidence from a heat flux transect across the upper limit of gas hydrate stability. *Geophysical Research Letters*, 44, 12,385–12,395. <https://doi.org/10.1002/2017GL076368>
- Pedley, K. L., Barnes, P. M., Pettinga, J. R., & Lewis, K. B. (2010). Seafloor structural geomorphic evolution of the accretionary frontal wedge in response to seamount subduction, Poverty Indentation, New Zealand. *Marine Geology*, 270(1-4), 119–138. <https://doi.org/10.1016/j.margeo.2009.11.006>
- Plaza-Faverola, A., Pecher, I., Crutchley, G., Barnes, P. M., Bünz, S., Golding, T., et al. (2014). Submarine gas seepage in a mixed contractional and shear deformation regime: Cases from the Hikurangi oblique-subduction margin. *Geochemistry, Geophysics, Geosystems*, 15, 416–433. <https://doi.org/10.1002/2013GC005082>
- Press, F. (1966). Section 9: Seismic velocities. *Geological Society of America Memoirs*, 97, 195–218. <https://doi.org/10.1130/MEM97-p195>
- Ranero, C. R., & von Huene, R. (2000). Subduction erosion along the Middle America convergent margin. *Nature*, 404(6779), 748–752. <https://doi.org/10.1038/35008046>
- Reyners, M. (1998). Plate coupling and the hazard of large subduction thrust earthquakes at the Hikurangi subduction zone, New Zealand. *New Zealand Journal of Geology and Geophysics*, 41(4), 343–354. <https://doi.org/10.1080/00288306.1998.9514815>
- Reyners, M., & McGinty, P. (1999). Shallow subduction tectonics in the Raukumara Peninsula, New Zealand, as illuminated by earthquake focal mechanisms. *Journal of Geophysical Research: Solid Earth*, 104, 3025–3034. <https://doi.org/10.1029/1998JB900081>
- Ruh, J. B., Sallarès, V., Ranero, C. R., & Gerya, T. (2016). Crustal deformation dynamics and stress evolution during seamount subduction: High-resolution 3-D numerical modeling. *Journal of Geophysical Research: Solid Earth*, 121, 6880–6902. <https://doi.org/10.1002/2016JB013250>
- Sacks, A., Saffer, D. M., & Fisher, D. (2013). Analysis of normal fault populations in the Kumano forearc basin, Nankai Trough, Japan: 2. Principal axes of stress and strain from inversion of fault orientations. *Geochemistry, Geophysics, Geosystems*, 14, 1973–1988. <https://doi.org/10.1002/ggge.20118>
- Stirling, M., McVerry, G., Gerstenberger, M., Litchfield, N., Van Dissen, R., Berryman, K., et al. (2012). National seismic hazard model for New Zealand: 2010 update. *Bulletin of the Seismological Society of America*, 102(4), 1514–1542. <https://doi.org/10.1785/0120110170>
- Taner, M. T., Koehler, F., & Sheriff, R. E. (1979). Complex seismic trace analysis. *Geophysics*, 44(6), 1041–1063. <https://doi.org/10.1190/1.1440994>
- Ten Veen, J. H., & Kleinspehn, K. L. (2003). Incipient continental collision and plate-boundary curvature: Late Pliocene-Holocene transtensional Hellenic forearc, Crete, Greece. *Journal of the Geological Society*, 160(2), 161–181. <https://doi.org/10.1144/0016-764902-067>
- Teyssier, C., Tikoff, B., & Markley, M. (1995). Oblique plate motion and continental tectonics. *Geology*, 23(5), 447–450. [https://doi.org/10.1130/0091-7613\(1995\)023<0447:OPMACT>2.3.CO;2](https://doi.org/10.1130/0091-7613(1995)023<0447:OPMACT>2.3.CO;2)
- Toda, S., Stein, R. S., & Lin, J. (2011). Widespread seismicity excitation throughout central Japan following the 2011 M = 9.0 Tohoku earthquake and its interpretation by Coulomb stress transfer. *Geophysical Research Letters*, 38, L00G03. <https://doi.org/10.1029/2011GL047834>
- Van Wagoner, J. C., Posamentier, H. W., Mitchum, R. M. J., Vail, P. R., Sarg, J. F., Loutit, T. S., & Hardenbol, J. (1988). An overview of the fundamentals of sequence stratigraphy and key definitions. In *Society of economic paleontologists and mineralogists special publications, sea-level changes: An integrated approach, Special Publications* (Vol. 42, pp. 39–44). Houston, TX: SEPM.
- Walcott, R. I. (1978). Geodetic strains and large earthquakes in the axial tectonic belt of North Island, New Zealand. *Journal of Geophysical Research*, 83, 4419–4429. <https://doi.org/10.1029/JB083iB09p04419>
- Walcott, R. I. (1984). The kinematics of the plate boundary zone through New Zealand: A comparison of short- and long-term deformations. *Geophysical Journal of the Royal Astronomical Society*, 79(2), 613–633. <https://doi.org/10.1111/j.1365-246X.1984.tb02244.x>
- Walcott, R. I. (1987). Geodetic strain and the deformational history of the North Island of New Zealand during the Late Cainozoic. In *Philosophical Transactions for the Royal Society of London. Series A*, 321(1557), 163–181.
- Wallace, L. M., Barnes, P., Beavan, J., Van Dissen, R., Litchfield, N., Mountjoy, J., et al. (2012). The kinematics of a transition from subduction to strike-slip: An example from the central New Zealand plate boundary. *Journal of Geophysical Research*, 117, B02405. <https://doi.org/10.1029/2011JB008640>
- Wallace, L. M., Beavan, J., McCaffrey, R., & Darby, D. (2004). Subduction zone coupling and tectonic block rotations in the North Island, New Zealand. *Journal of Geophysical Research*, 109, B12406. <https://doi.org/10.1029/2004JB003241>
- Wallace, L. M., Reyners, M., Cochran, U., Bannister, S., Barnes, P. M., Berryman, K., et al. (2009). Characterizing the seismogenic zone of a major plate boundary subduction thrust: Hikurangi Margin, New Zealand. *Geochemistry, Geophysics, Geosystems*, 10, Q10006. <https://doi.org/10.1029/2009GC002610>

- Wallace, L. M., Webb, S. C., Ito, Y., Mochizuki, K., Hino, R., Henrys, S., et al. (2016). Slow slip near the trench at the Hikurangi subduction zone, New Zealand. *Science*, *352*(6286), 701–704. <https://doi.org/10.1126/science.aaf2349>
- Wang, H., Crutchley, G. J., & Stern, T. (2017). Gas hydrate formation in compressional, extensional and un-faulted structural settings— Examples from New Zealand’s Hikurangi margin. *Marine and Petroleum Geology*, *88*, 69–80. <https://doi.org/10.1016/j.marpetgeo.2017.08.001>
- Wang, K., & Bilek, S. L. (2011). Do subducting seamounts generate or stop large earthquakes? *Geology*, *39*(9), 819–822. <https://doi.org/10.1130/G31856.1>
- Webb, T. H., & Anderson, H. (1998). Focal mechanisms of large earthquakes in the North Island of New Zealand: Slip partitioning at an oblique active margin. *Geophysical Journal International*, *134*(1), 40–86. <https://doi.org/10.1046/j.1365-246x.1998.00531.x>
- Woodcock, N. H., & Fischer, M. (1986). Strike-slip duplexes. *Journal of Structural Geology*, *8*(7), 725–735. [https://doi.org/10.1016/0191-8141\(86\)90021-0](https://doi.org/10.1016/0191-8141(86)90021-0)
- Yielding, G., Badley, M. E., & Freeman, B. (1991). Seismic reflections from normal faults in the northern North Sea. *Geological Society, London, Special Publications*, *56*(1), 79–89. <https://doi.org/10.1144/GSL.SP.1991.056.01.06>
- Yu, Y., Kelley, C. L., & Mardanova, I. M. (2015). *U.S. patent no. 9,105,075*. Washington, DC: U.S. Patent and Trademark Office.
- Zoback, M. L., Thompson, G. A., & Anderson, R. E. (1981). Cainozoic evolution of the state of stress and style of tectonism of the Basin and Range province of the western United States. *Philosophical Transactions of the Royal Society of London, Series A*, *300*(1454), 407–434.